Parameter Identification and Modelling
for the Prediction of Voltage Distortion

by

Christopher Reed Laughman

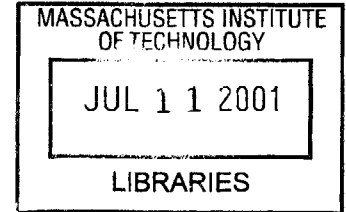S.B., Massachusetts Institute Of Technology, June 1999

Submitted to the Department of Electrical Engineering and Computer Science
in partial fulfillment of the requirements for the degree of

Master Of Engineering in Electrical Engineering

at the

MASSACHUSETTS INSTITUTE OF TECHNOLOGY

June 2001

Author ....
Department of Electrical Engineering and Computer Science
May 28, 2001

Certified by.............................
Steven B. Leeb
Associate Professor
Thesis Supervisor

Certified by...
Steven R. Shaw
Assistant Professor, Montana State University
Thesis Supervisor

Certified by.........
Leslie K. Norford
Associate Professor
Thesis Supervisor

Accepted by......
Arthur C. Smith
Chairman, Department Committe on Graduate Theses

Parameter Identification and Modelling

for the Prediction of Voltage Distortion

by

Christopher Reed Laughman

Submitted to the Department of Electrical Engineering and Computer Science
on May 28, 2001, in partial fulfillment of the
requirements for the degree of
Master Of Engineering in Electrical Engineering

Abstract

This thesis presents a set of techniques for predicting point-of-load voltage distortion on the electric utility and in the electrical system of the automobile. Continuous-time models for the impedances of both the electric utility and the automobile chassis are constructed, and parameter estimates for continuous-time and discrete-time versions of these models are obtained via linear and nonlinear least-squares minimizations. Experimental techniques required to implement these methods are discussed, and the results of applying the techniques for predicting voltage distortion in both systems are demonstrated.

Thesis Supervisor: Steven B. Leeb
Title: Associate Professor

Thesis Supervisor: Steven R. Shaw
Title: Assistant Professor, Montana State University

Thesis Supervisor: Leslie K. Norford
Title: Associate Professor

Acknowledgments

I would like to thank Professor Steve Leeb for his advising and assistance over the last four years, and specifically over the last two while the research for this thesis was being performed. His encouragement and patience are inspiring, and my MIT experience has been greatly enhanced because of the time he has spent helping me down the path to becoming an engineer.

A great debt is also owed to Professor Steven Shaw, without whom I would still probably be trying to figure out how to make accurate measurements. His sage advice on all matters, technical and non-technical, has taught me volumes on how to approach and solve problems in a rigorous way.

Thanks also to Professor Les Norford for providing many helpful comments on this thesis as it turned from a odd conglomeration of ideas into a coherent document.

My officemates and comrades in research, Steve Shaw, John Rodriguez, Joshua Phinney, and Ernst Scholtz, deserve thanks for their friendship and support over the course of this research. Their understanding ear was always helpful when simulations wouldn't converge and measurements didn't make any sense; the simulations and measurements didn't work any better, but at least they were enjoyable.

I would like to thank my many roommates and friends who have dragged me out of the lab and forced me to have a life over the last two years. They are individually and collectively responsible for making sure that I can still function (in some manner) as a member of society, and I am endlessly grateful for their support.

Lastly, I would like to thank my family for being there for me through the many ups and downs over the last six years. They have provided me with a sense that there exists some reality outside of this insane college life, and never expressed any doubt even though I have said that I would be done in about a week every Sunday for the past year. This thesis is dedicated to them.

Contents

List of Figures

Chapter 1

Introduction

One area of increasing concern in both industry and consumer circles during the late 1990's and early 2000's has been that of power consumption. As made clear by incidents such as the Winter 2001 power crisis in California, the present demand for power often meets or exceeds the ability of the present power generation infrastructure. Though this fact has innumerable effects, one consequence of particular interest is the restriction that the utility must now place on maximum power consumption. Facilities, such as assembly plants and office buildings, are presently being billed on both a steady-state and a peak power basis. If an assembly plant experiences a spike in its power consumption that exceeds its peak power rating, it is penalized by the utility through a system of extra charges. These monetary penalties can be significant; one representative penalty charge is $10 per kilowatt hour.

It naturally follows that a great deal of consideration is currently being given, on the part of both the loads and the utility, to methods by which it might be possible to forecast and avoid these troublesome power spikes. Technology presently exists([8]) which can, by examining only the current and voltage where a facility connects to the electric utility, disaggregate the individual loads turning on and off within that facility. This capability of identifying the present state of individual loads, coupled with the ability to predict the effects that other loads will have if connected to the electrical system, would allow both the user and the utility to understand and control the level of power at any given time.

Power spikes are also studied on a smaller scale in the design of most electronic systems. These spikes occur in many systems, such as motors and heating systems, due to the large currents required for the system in a steady-state condition to respond to a step command.

Large transient currents can cause problems when they flow through impedances which are small enough to neglect in steady-state operation, but large enough to produce significant voltage transients. These voltage transients are often not predicted, and are occasionally big enough to damage components which were chosen with tolerances corresponding to the system's desired steady-state behavior. By predicting this behavior in systems where the voltage transients are poorly understood at this time, a more accurate picture of the system's behavior can be obtained.

The goal of this thesis is the prediction of voltage distortion with the knowledge of the time characteristics of the current transient. The predictions will be obtained in two systems: the electric utility and an automobile. By understanding and predicting transient behavior in these systems, improvements might be made that have wide-ranging impact due to the role of these systems in modern society. The ability to predict the transient interactions between electrical loads will also enable users to avoid power spikes in these systems. In addition, these two entities together represent a larger class of systems than each individually, as voltage distortion prediction techniques will be developed in both AC and DC contexts.

1.1   Background

When examined from an overarching perspective, the process of predicting voltage distortion can be summarized as a problem for which its is necessary to create a model.

Before embarking on the task of predicting voltage distortion in both the electric utility and automobile, it is necessary to make a few general comments with regards to the process of system identification. The task of using prefabricated models (*simulation*) is often emphasized over that of constructing new models (*system identification*), since the engineer's task usually consists of constructing a new system from predefined building blocks. During simulation, a model operates upon a specified input to arrive at an estimate for the quantity of interest without the implication that its parameters will be modified at any future time. It is usually assumed that the model is a self-contained entity that requires an input and/or an initial state, as well as time, in order to produce the desired output.

In comparison, the process of system identification finds a model which serves as an accurate mapping between input and output. This process can be viewed as a type of

inverse problem to that of simulation, as the normal process of using an input and a model to generate an output has to be inverted so that the input and the output are used to generate a model. In the case at hand, the process of system identification involves identifying an impedance: a mapping that will produce a voltage estimate from a given current excitation. The impedances being identified are those of the electric utility and the automobile's chassis.

System identification is inherently more complicated than simulation, as the fundamental goal of system identification is the creation of a mapping between input and output. Simulation is nominally a one-step process, for it only requires that the model operate on a given input to produce an output. System identification, on the other hand, is a two-step process. The first step, referred to as characterization, consists of the selection of an input/output mapping (*model*) and determination of the set of parameters (*parameter estimation*) that governs a relation between the actual input and output data.

Obtaining an identified model is not necessarily the final step, as the accuracy of the mapping must be verified before the model can be finalized. This process of verification is referred to as *cross-validation*, and consists of comparing the result of a simulation to the experimentally generated output. If the residual produced by the cross-validation does not conform to the desired specification, the process of system identification returns to the modelling or parameter estimation steps. One common pitfall in the process of system identification is that the system is characterized, only to find out that even the best set of parameters for the selected model does not accurately represent the system under consideration. Only after the system is characterized using one set of data and then cross-validated with another (in order to avoid pathologically good fits to an otherwise poor model), can the model be used for the purposes of simulation.

$$x \longrightarrow \boxed{\bar{F}(x,t;\mu)} \longrightarrow y \qquad\qquad x \longrightarrow \boxed{F(x,t;\hat{\mu})} \longrightarrow \hat{y}$$
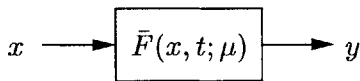
Figure 1-1: The system $\bar{F}$ maps the measured input x to the measured output y.
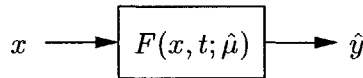
Figure 1-2: The system F serves as an approximation to $\bar{F}$, and maps the measured input x to a predicted output $\hat{y}$.

Rather than leave the entire explanation process to the vagaries of textual description, it is helpful to explain the relationship of simulation and system identification in a mathematically-oriented context. Suppose that some system $\bar{F}$ exists, as in Figure 1-1, and

that it is necessary to construct a model for this system. While it is possible to examine the input x and the output y, only approximations of the relation $\bar{F}$ between the two can be constructed. The goal of system identification is therefore the production of a system F that can use the input x to generate a prediction $\hat{y}$ in such a way that the difference $(y - \hat{y})$ is minimized. This approximate system is represented in Figure 1-2.

The close ties between system identification and simulation should be acknowledged, and can be seen through the process by which F is identified. The system F must first be characterized with one set of data (x_c, y_c), so that F and $\hat{\mu}$ may be obtained. This model is then cross-validated with another set of data (x_v, y_v) to ensure that the model F is correct and that the set of parameters $\hat{\mu}$ produce an estimate $\hat{y}$ which is closest to y, according to some criterion. Once this has been accomplished, the system $F(x, t; \hat{\mu})$ is said to represent $\bar{F}(x, t; \mu)$ accurately, and may be used for the purposes of simulation and prediction.

Though the general structure of system identification has been discussed, there are a few subtle points which require emphasis. One of the important details which should not be overlooked is that the structure of the model being parametrized is strongly dependent upon the manner with which the modelled system is excited during identification. This idea is presented most coherently by an example; consider the problem of identifying the system shown in Figure 1-3.
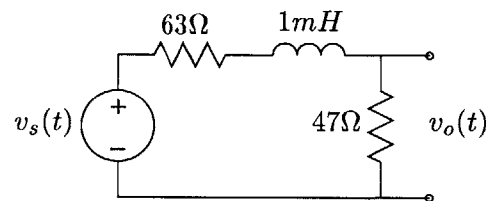
Figure 1-3: A passive network used to illustrate the connection between the creation and the use of a model.

By measuring the response of the above system on differing time scales, its behaviors can be made to look very dissimilar. Figures 1-4 and 1-5 make this fact clear.

If the system is identified on a timescale of $150\mu s$, the effect of each of the elements can be observed (Figure 1-4). If the system were examined by using a different timescale, however, this would not be as apparent; consider measuring the system on a timescale of $150ms$. By switching timescales (Figure 1-5), the model would probably not include a

13
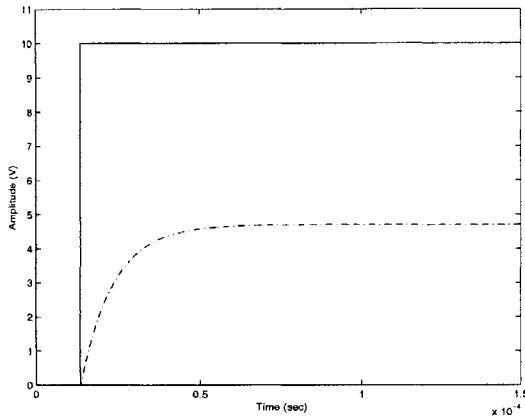
Figure 1-4: Response of $v_o(t)$ (dotted line) to a $10V$ input step (solid line) over a time scale of $150\mu s$.
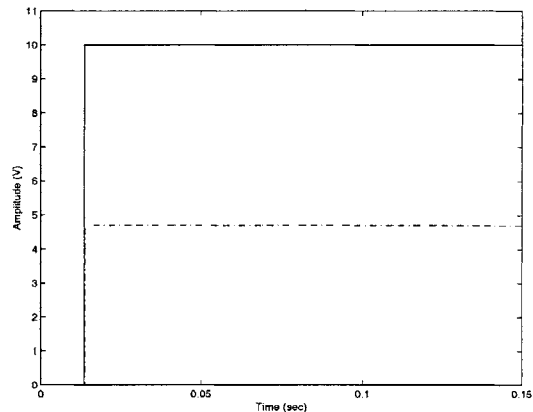
Figure 1-5: Response of $v_o(t)$ (dotted line) to a $10V$ input step (solid line) over a time scale of $150ms$.

term corresponding to the inductance. More importantly, it would be impossible to find a value for this parameter which corresponded to any physically meaningful component if an inductance term were included in the model. The model's dependence on the type of excitation therefore requires that the inputs used for the purposes of identification and cross-validation be similar to the inputs to be used with the resulting model.

Along the lines of the last example, it is also essential that the experimental setup during the data collection for the system identification process be similar to the setup under normal operating conditions, as used for prediction. The goal of the parameter estimation step is finding parameters of the model which force the output of the model to resemble the observed output as closely as possible. In choosing the parameters of the model under this constraint, the system identification process will often capture information from the experimental setup as well as from the system.

This can be seen via a simple extension of the previous example. Consider the connection of an oscilloscope to the previous system, as displayed in Figure 1-6. The model for the system will be very similar to that shown in Figure 1-4 if the characterization data are taken with $R_s = 1M\Omega$ over a time scale of $150\mu s$. If the resulting model (with a correctly identified set of parameters) is then tested with the R_s of the oscilloscope changed to 50Ω, the model output and the oscilloscope output will differ by almost a factor of 2. This demonstrates the necessity of matching the experimental setup during system identification

14
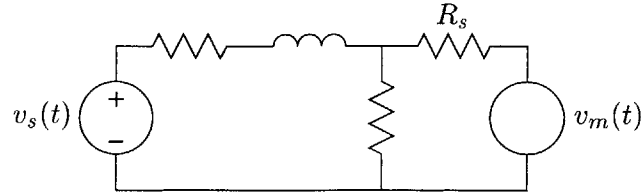
Figure 1-6: A passive network which illustrates the influence of measurement on the parameters of a model.

as closely as possible to the setup for prediction.

A considerable amount of work has already been done on modelling the electric utility [9]. The problem pursued in [9] shares many similarities to the challenge posed in this thesis, but there are a few differences. In particular, the approach taken in [9] is that an isolation transformer is connected to the standard utility connection so that the output impedance of this transformer is modelled rather than the direct utility. This was performed so that the parameters of the transformer might be characterized separately from the experiment, as a sort of intermediate check before directly modelling the utility's impedance. This thesis does not pursue this intermediate verification step, but instead characterizes the utility directly.

Furthermore, the method for exciting transients on the utility in [9] is different from the method pursued in this thesis. Lepard chose to excite transients by connecting capacitors across local wall outlets, and then measuring the parameters of the utility from the resulting damped oscillations in voltage and current. A number of capacitors were used to characterize the utility over a range of frequencies. In comparison, the technique exploited in this thesis drew a particular command current from the wall, and then used the resulting current and voltage waveforms to estimate the parameters of the utility. A continuation of the work performed in [9] is given in [13].

In comparison to the work previously done on the electric utility, little work on directly modelling the automobile chassis has been done. A great deal of work has been done on issues closely related to the prediction of voltage distortion in the automobile, however. Extensive research has been performed of the behavior of electric fields in conducting sheets, specifically in reference to the eddy current losses in cylindrical shields [6] and in transformer cores [1]. Furthermore, the prediction of voltage distortion in aircraft has been widely

studied in order to prevent accidental faults [5].

1.2 Outline

This thesis proceeds by following the system identification process for the electric utility and the automobile chassis in parallel. Chapter 2 is dedicated to the step of modelling. The electric utility is modelled first via physically-based reasoning, and this model is then refined by using experimental data. The automobile chassis is then modelled by building upon some of the intuition obtained from the utility; experimental findings are used to refine this model as well.

A selection of continuous-time and discrete-time parameter estimation methods are discussed in Chapter 3. The continuous-time λ method and discrete-time ARMAX method are explained in general, and they are then applied to the model of the electric utility which was developed in Chapter 2. Following this discussion, the idea of nonlinear least-squares minimization is summarized as it applies to the parameter identification of the automobile chassis, and the continuous-time λ method is discussed briefly in the context of the automobile chassis before a specific discrete-time identification technique is introduced and presented in detail.

Chapter 4 is concerned with the experimental verification of the techniques discussed in Chapters 2 and 3. The data collection hardware and preprocessing required for the utility are presented first, followed by the results of applying the aforementioned system identification techniques to the electric utility. A similar tack is taken with the automobile; a discussion of the hardware and experimental setup for the automobile chassis is presented, and the results of applying the system identification techniques are analyzed. Chapter 5 contains the conclusions reached in the course of this research, as well as suggestions for further work.

Chapter 2

Model Selection

One logical way to approach the problem of predicting voltage distortion is by developing a functional relationship between the quantity to be predicted and the information upon which the prediction is based. As discussed in Chapter 1, the input/output relationship can be expressed as a mapping expressed by some function $F(x, t; \hat{\mu})$. The goal of this chapter is the determination of the models F of both the electric utility and the automobile chassis which can mathematically relate the current to the voltage distortion.

This modelling process is largely the same in the cases of both the electric utility and the automobile chassis. Initially, intuition and reasoning based upon the physical layout of the system are used to obtain an approximate model. The preliminary model is then refined via theory and preliminary validation tests, which will qualitatively test the degree to which the model characterizes the system accurately. As the model for the chassis builds upon some aspects of the utility, the model for the electric utility is presented first.

2.1 The Electric Utility

Consider the standard manner in which individual loads are connected to the electric utility and draw currents, such as $i_1(t)$ or $i_n(t)$, as illustrated by Figure 2-1. In this context, the electric utility is referred to as the voltage source seen by the consumer inside a building; this voltage source could be referred to as the wall voltage equally well. Since this voltage source has a nonzero impedance, the currents drawn by the individual loads will produce a voltage drop across the impedance of the utility, and this voltage drop will in turn affect the other loads. The goal of this thesis is therefore the prediction of this effect; that is to say, we seek
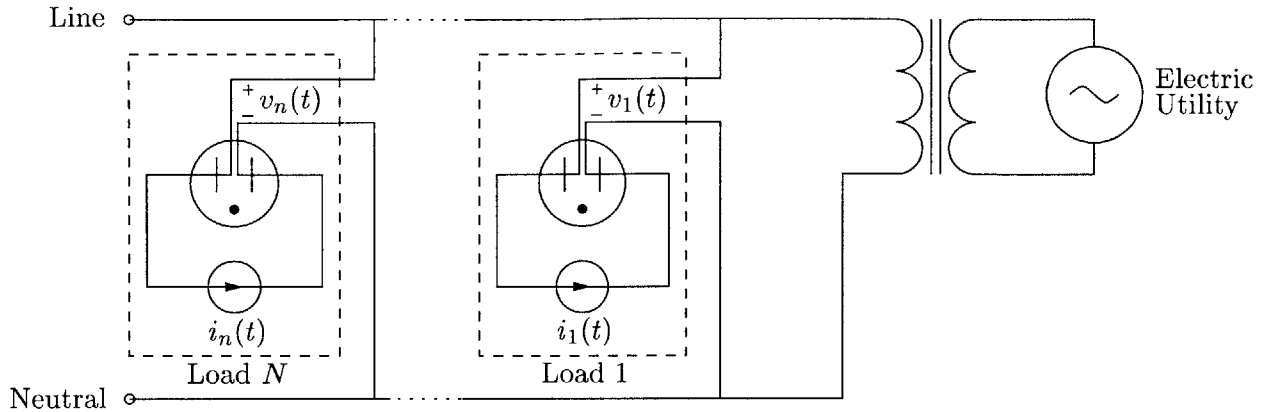
Figure 2-1: A distribution-level model of the connection of user-level loads to the electric utility.

to predict the effect of the current i_1 on the line voltage seen by other loads (e.g. v_n). This is commonly known as the prediction of point-of-load voltage distortion. This figure suggests that the impedance seen by the individual loads is due to the components comprising the connection to the power distribution network, such as the transformer and the set of cabling and protection devices. The transformer serves to modify the transmission voltage down to the voltage at which it is used, such at the standard 110 V_{rms} in most residential homes; the other impedances allow the power to be used where it is needed.

One simple model which accurately describes the behavior of the system is shown in Figure 2-2.
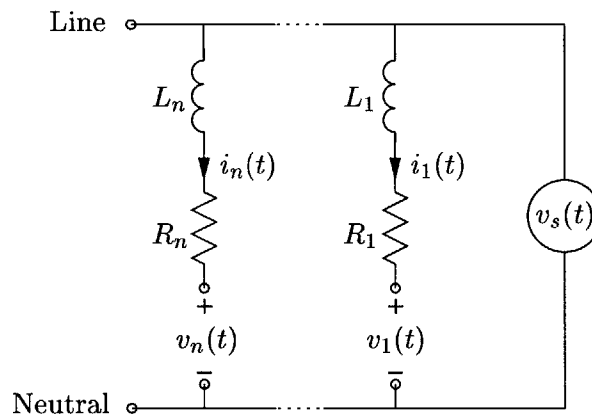
Figure 2-2: A schematic diagram describing the impedance of the electric utility seen from a point-of-load perspective.

The L_i describe the frequency-dependent behavior of the transformers and frequency dependent elements upstream from the load voltage, while the R_i describe such effects as the resistance of the distribution wire, the impedance of the protection devices, and the resistance of the transformer windings. It is important to note that each node will see a slightly different impedance looking into the source, due to the variation in the amount of cabling between the transformer and each particular outlet.

One crucial simplifying assumption was made in order to render the goal of voltage prediction tractable; it is assumed that the wall voltage is invariant to current perturbations on the time scale of the transients drawn by the individual loads. This property of the voltage source is referred to as being stiff. In other words, it is obvious that the wall voltage will be affected by such factors as power-factor-correction capacitors across upstream transformers, upstream voltage distortion, and the aggregate current drawn by loads at any given point in time. The time scale over which all of these factors have an effect, however, is much larger than the time scale of the transient perturbations which cause local voltage distortion. Furthermore, the service one step upstream (e.g. beyond the closest transformer) is usually capable of providing ten times the current that any individual load will draw. These two facts in combination justify the approximation that the voltage source is stiff. Additionally, we are assuming that no other current perturbations, or transients, are taking place while the one of interest is occurring. This has been found to be generally true; a similar assumption is used in [2], [12], and [13].

Consider the kth connection to the system described in Figure 2-2. By recording the waveforms $v_s(t)$, $v_k(t)$, and $i_k(t)$, it is possible to estimate the parameters R_k and L_k of the point-of-load model of the utility. While the process of capturing $v_k(t)$ and $i_k(t)$ is relatively straightforward, it is generally much more difficult to measure $v_s(t)$. Under the assumption that $v_s(t)$ is stiff and that most loads are in the steady state,

$$v_s(t) \approx v_s(t - nT) \tag{2.1}$$

where nT is a small multiple of the line voltage's fundamental period. This is again principally taking advantage of the assumption that $v_s(t)$ generally does not change from cycle to cycle, in comparison to the time scale on which the current transients are occurring.

With this information, it is possible to construct an approximation $\hat{v}_s(t)$ to $v_s(t)$ by

measuring $v_k(t - nT)$ while $i_k(t - nT) = 0$, and using it as an approximation for $v_s(t)$ when $i_k(t) \neq 0$. In other words,

$$\hat{v}_s(t) = v_k(t - nT), \quad \text{with } i_k(t - nT) = 0. \tag{2.2}$$

This observation could be used experimentally by measuring $v_k(t)$ for a few periods of T before and after the test current $i_k(t)$ is applied. Note that this approximation would not be possible if the voltage source were susceptible to disturbances on the order of the current transients. This would effectively rule out this method of estimating $v_s(t)$ during a current transient.

The effect of unmeasured steady-state load currents must be considered in seeking to include as many experimental constraints in the model as possible, as the requirement of turning all non-characterizing loads off in order to characterize the impedance of the utility is clearly an unrealistic requirement. Under the previously stated assumption that there is a linear operator H which relates the current in the utility $i(t)$ to the voltage $v(t)$, it is possible to show that an unmeasured steady-state current can be accommodated. This scenario is illustrated by Figure 2-3.
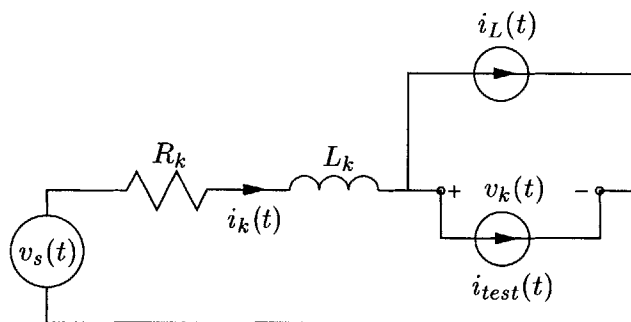
Figure 2-3: A schematic description of the experimental condition in which an unmeasured steady-state current is present as well as the test current excited for identification purposes.

In the absence of $i_L(t)$, the equation

$$\begin{aligned} Hi(t) &= v(t) \\ &= v_s(t) - v_k(t) \end{aligned} \tag{2.3}$$

is used to estimate the parameters of the system. If an unmeasured load current is in-

troduced at node k, Kirchoff's current law now prescribes a different relation between the currents, i.e.

$$i_k(t) = i_L(t) + i_{test}(t) \qquad (2.4)$$

This has two related consequences. The first is that Equation 2.2 must be modified to account for the effect of this steady-state current, becoming

$$\hat{v}_s(t) = v_k(t - nT), \quad \text{with } i_k(t - nT) = i_L(t - nT). \qquad (2.5)$$

The other consideration is that the voltage drop across the modelled impedance is proportional to the current running through it; the portion of this drop which is due to $i_M(t)$ must be proportional to the difference between the total current passing through it when $i_{test}(t)$ is active, and the steady-state current $i_L(t)$. In other words,

$$
\begin{aligned}
H i_{test}(t) &= \hat{v}_s(t) - v_k(t) & (2.6) \\
&= (v_s(t - nT) - H i_L(t - nT)) & \\
&\quad - (v_s(t) - H(i_L(t) + i_{test}(t))) & (2.7)
\end{aligned}
$$

This shows that an unmeasured load current $i_L(t) = i_L(t - nT)$ cancels itself on both sides of the equation and therefore has no effect on the problem. There are some loads which might be strongly perturbed during the characterization, such as capacitors. In order to avoid collecting faulty data, these loads should be disconnected during the characterization.

2.1.1 Frequency Dependence of R_k

The model illustrated in Figure 2-2 is accurate in the sinusoidal steady state for one given frequency. This is of limited use, however, as the voltage transients which serve as the model input contain frequency information between the fundamental of the electric utility (60Hz) and the sixteenth harmonic. As this model was tested in an experimental setting, it was found that the resistances R_k were observed to increase nonlinearly as the frequency of excitation f was varied. The preliminary model therefore had to be modified. This observation could result from the manifestation of a few different phenomena; some explanations include the skin effect on the wires or the eddy currents induced in adjacent conductors.

The change in resistance due to the skin effect in a cylindrical conductor is given in [4];

22

for $x \ll 1$ ("low" frequencies) the expression for the resistance is

$$\frac{R}{R_0} = 1 + \frac{x^4}{192} \tag{2.8}$$

where $x \propto \sqrt{f}$. The constant of proportionality (given explicitly in [4]) is related to the physical properties and geometry of the conductor, while R_0 is the DC resistance.
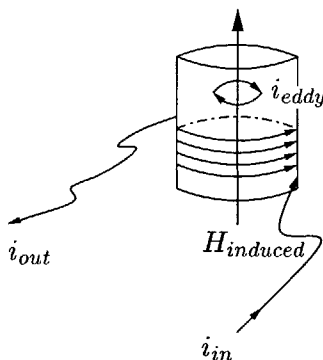
Figure 2-4: Illustration of the electromagnetic fields present in a transformer.

Understanding the effect of eddy currents induced in conductive materials located in close proximity to the current wires is also useful. The geometric relationship of these eddy currents to the excited currents are shown in Figure 2-4. The current flowing through the windings of the transformer is denoted by i_{in} and i_{out}; Maxwell's equations dictate that this current will induce a magnetic field ($H_{induced}$) in the core and eddy currents (i_{eddy}) that flow within the core. The changes in the effective resistance of the winding itself are again given in [4]; for $\theta \ll 1$

$$R \approx R_0 + 2\pi f L_0 \frac{\theta^2}{6} \tag{2.9}$$

In this equation, $\theta \propto \sqrt{f}$ and R_0 is equal to the DC resistance of the winding. The constant of proportionality is geometry and material dependent as in Equation 2.8 and can be analytically derived for certain geometries.

Assuming that the constants relating x and θ to $\sqrt{f}$ satisfy the necessary conditions, Equations 2.8 and 2.9 suggest that both the skin effect and induced eddy currents can be modelled by adding the following frequency dependent term to the resistive component of the utility model:

$$R(f) = R_0 + \delta f^2 \tag{2.10}$$

23

By collecting data at a number of different frequencies, a least-squares solution for 2.10 can be found. At last, then, a model for the electric utility can be stated; this 3-parameter model looks like

$$\frac{V_M}{I_M}(s) = R_0 + Ls + \delta s^2 \qquad (2.11)$$

This model certainly signifies progress toward the eventual goal of predicting voltage distortion, but it is by no means the end of the problem. The next step towards the goal is that of finding R_0, L, and δ in a repeatable and reliable manner. This subject is broached in Chapter 3.

2.2 The Automobile Chassis

In comparing the two systems to be modelled, it might appear that the process of modelling an automobile chassis would be much easier than that of the electric utility. This is true in some senses; many of the difficulties encountered in modelling the electric utility, such as the inability to directly measure the voltage across the modelled impedance as well as accounting for unmeasured steady-state currents, are not encountered in the experimental conditions under which the chassis is modelled.

The model of the chassis and the process by which the parameters are obtained from the data are therefore very straightforward. Measurements of the current flowing into the chassis and the voltage across the chassis are obtained, and the parameters μ of the model

$$v(t) = z(\mu)i(t) \qquad (2.12)$$

are selected so as to closely model the input/output relations manifested by the experiments. Given that the input and output variables are explicitly available, the only remaining question is that of choosing an appropriate model. This question is addressed in the following section.

2.2.1 Dominant Pole Model

Figure 2-5 illustrates the experimental setup from which data will be collected, and serves to tie the abstract goal of predicting voltage distortion to a concrete physical realization. The model being generated will predict the voltage waveform between any two of the four nodes

based upon the current injected into nodes 1, 2, or 3. It is significant that the current is not injected into node 4, as the current as always is returned from that node. This constraint was imposed upon the model because the bonding strip which connects the chassis to the battery serves as an important component of the impedance being measured. Though
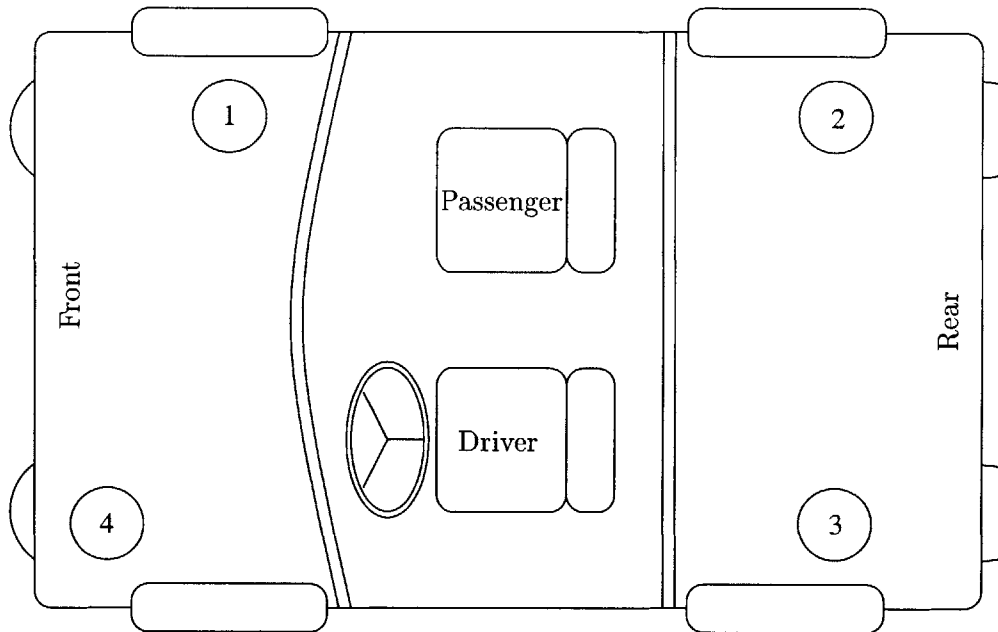
Figure 2-5: The experimental layout of the automobile chassis as modelled in this thesis.

the chassis contains numerous welds and connections between steel of different structures and thicknesses, one suggestive approximation is that it roughly possesses the physical and electrical properties of one highly deformed steel sheet. This simple fact suggests one powerful technique for accomplishing the goal; with an appropriate model of the steel, the behavior of this system could therefore be governed by a set of transfer functions, with the current injected at one port, and the voltage measured across another port. This model is somewhat lacking in its generality, due to the fact that the number of models required to predict the response at an arbitrary output port from an arbitrary input port is equal to the product of the possible number of input ports and the possible number of output ports. While this is a definite drawback, this method remains appealing because it would require only one model and twelve specific sets of parameters.

This fact can be clearly illustrated by considering the following experiment: a measured current is injected into node 1, and the four voltages along each adjacent side are also

measured. Given a general transfer function model which maps the current flowing through a steel sheet to a voltage measured across any two points on that sheet, it is possible to find four different sets of parameters of the general transfer function, which correspond to the four specific transfer functions relating the injected current to the measured voltages.

The task of modelling the car can therefore be divided into two separate tasks: constructing and validating a model for a sheet of steel, and then verifying the fact that the car chassis can indeed be modelled as such. The first element in this process is not very straightforward, however, as the analytical process for deriving the general transfer function which serves to model the impedance of a steel sheet is much more complicated than the analogous process for a transformer. By simply comparing the interactions of electromagnetic fields in Figures 2-4 and 2-6, it is apparent that the driving current, magnetic field, and induced eddy currents are much more coupled in the steel sheet than the same variables in the transformer model. Due to this added complexity, the model of the steel sheet is based
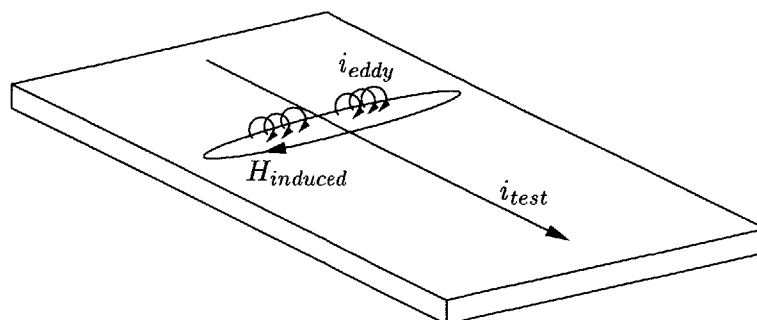
Figure 2-6: A diagram of the electromagnetic fields present in a sheet of steel.

more upon physical intuition than direct modelling. Simply put, the proposed electrical model for a steel sheet is a resistor and an inductor in series, so that the transfer function of the steel sheet looks like

$$\frac{V_{steel}(s)}{I_{steel}(s)} = R_0 + Ls \qquad (2.13)$$

The physical intuition for this model is based upon two observations, the first of which is simply the fact that the steel sheet, as a nonideal chunk of metal, must have some nonzero DC resistance. The second observation is that the time-varying current in the steel must, by Maxwell's equations, create a time-varying magnetic field, and that the interaction of

that magnetic field with the current will produce an inductive effect. This model for the steel of the automobile chassis will be referred to as the dominant pole model, for it models the complex behavior reflected in Figure 2-6 by making the assumption that the pole due to the inductance is located at a low frequency with respect to the collection of poles that arise from second order effects in the steel sheet. This pole is therefore said to dominate the frequency response.

This approximation is supported by experimental data as well as physical intuition; as such a check, the circuit shown schematically in Figure 2-7 was constructed, where a uniform section of steel sheet in the trunk of the car was used as the test jig. This particular piece of steel was selected because the magnetic permeability of steel is highly dependent on the production process, and it was desired that the test resemble the final experimental setup as closely as possible. It stands to reason through examination of this plot that the
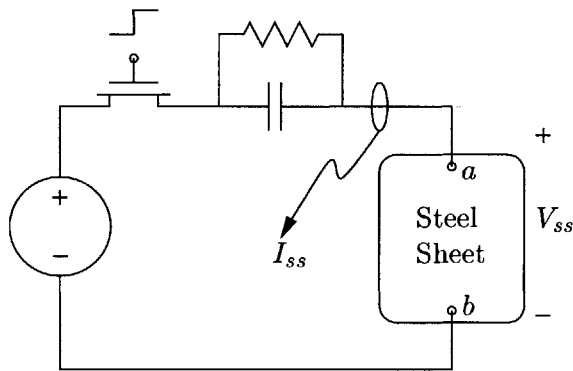
Figure 2-7: Experimental setup used to verify the accuracy of the $R + Ls$ model of a sheet of steel.
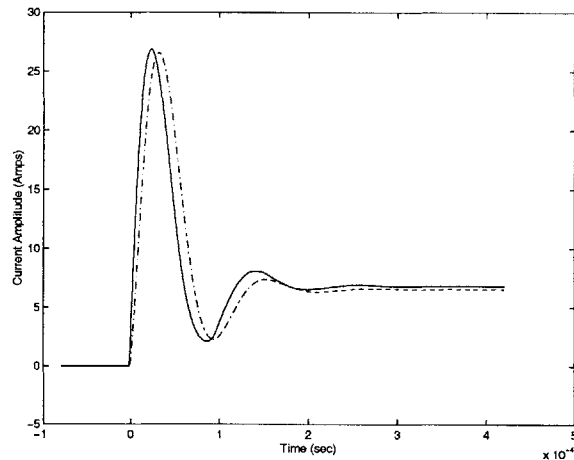
Figure 2-8: Plot of the measured and predicted currents flowing through the steel sheet. The solid line represents the measured current, while the dotted line represents the prediction.

behavior of the steel sheet would govern the response of the system to a step in voltage. As is evident from significant ringing displayed in the plot of the resulting current in Figure 2-8, the system is indeed affected by the presence of both inductive and resistive elements. The parameters which verify the model for the steel sheet were obtained by using methods discussed in detail in Chapter 3.

2.2.2 A Refined Model of the Car

While one model of a steel sheet has been proposed and validated, the claim that an automobile chassis can be successfully modelled as a steel sheet has yet to be experimentally demonstrated. In order to verify the proposition, an experimental setup was constructed in a similar manner to that described in Figure 2-7, with terminals a and b being hooked up to the chassis via to nodes 2 and 4, respectively. Indeed, when the model from Equation 2.13 was used to characterize the electrical behavior of the chassis (again using the parameter estimation methods of Chapter 3), it was found to perform poorly. This fact is immediately apparent when comparing the two plots in Figure 2-9.
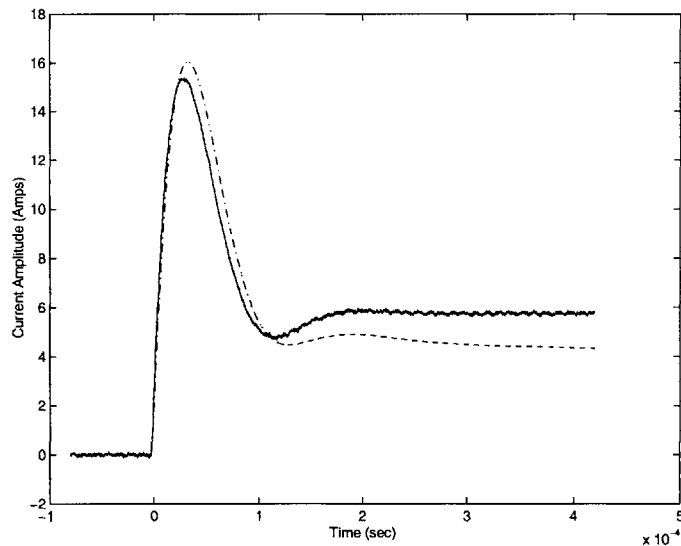
Figure 2-9: Plot illustrating the inability of the $R + Ls$ model to describe the electrical behavior of the entire chassis. The measured current is denoted by a solid line, while the prediction is denoted by the dashed line.

Upon further reflection, the disparity between the behavior of a single steel panel and the entire automobile chassis is not extremely surprising. Many possible explanations for this difference exist. One reasonable justification is based upon the observation that the chassis is much more complex than a single sheet of steel, as it is composed of many different pieces of steel joined by a set of spot welds. Furthermore, the electrical behavior of two welded sheets of steel is not equivalent to the behavior of one large uniform steel plate; possible differences include the nonuniformity of current density in the welded sheets as well as nonlinear effects introduced from the variable current density. Research has not

been performed to pinpoint the exact cause for the failure of the original model, but the need to refine the model to account for the shortcomings of the present model is apparent.

One tactic which was successfully employed in refining the model takes a popular approach to model refinement: as it is likely that the problems with the model stem from a poor approximation of the behavior of the electromagnetic field present, more degrees of freedom were added to the model in order to capture this behavior. These degrees of freedom were added by changing the model of a chassis from a single sheet of steel to grid of an interconnected network of steel plates, each of which is modelled by the experimentally validated model of a steel sheet. This model is best described pictorially in Figure 2-10.
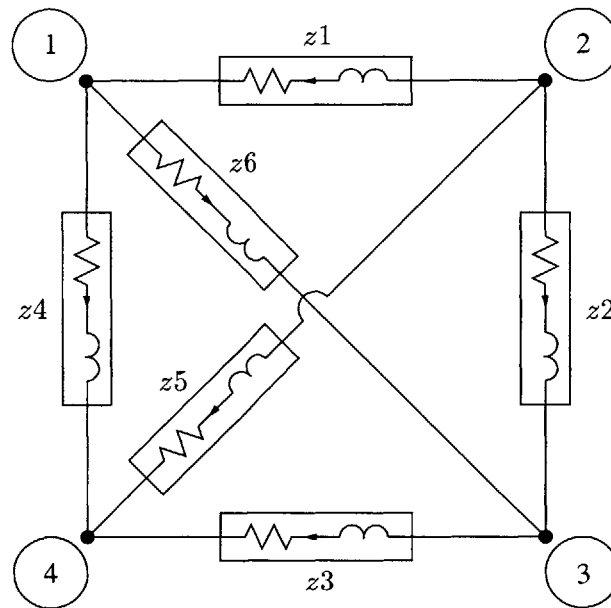
Figure 2-10: A refined electrical model of the automobile chassis, representing its nature as an interconnection of steel panels.

With the decision to add extra terms to the model comes a much more subtle question: how many extra terms should be added? In other words, the question now posed regards the number of steel plates which comprise the model of the chassis. A great deal of work has been done in the study of optimal methods to add terms to models, a topic which is known generally as model order determination. Though it is possible to use many techniques to choose an optimal number of terms, this thesis took a more pragmatic approach and simply used as many steel plates as were necessary to fully connect together all of the observed nodes (resulting again in Figure 2-10). This was done for two reasons, the first being that a

visual inspection of the chassis does not suggest any particular branches of the model which should obviously be removed. All of the branches were also kept simply because problems in obtaining parameter estimates were not encountered with this model, and it was therefore not modified any further.

Though this new model is able to capture the behavior of the automobile chassis more accurately, the modifications also introduce a set of issues which must be accommodated. Most significant among these issues is the fact that the current flowing through each branch of the model can no longer be directly measured. One of the reasons that the original model was attractive was the possibility of measuring the current through and voltage across the impedance at all times, so that a relation only needed to be constructed to relate the two variables. By changing models, this fact has ceased to be true; an examination of the experimental setup as it pertains to the new model Figure 2-11 will illustrate the new challenge posed by the change. The process of collecting data requires that a current i_{test1},
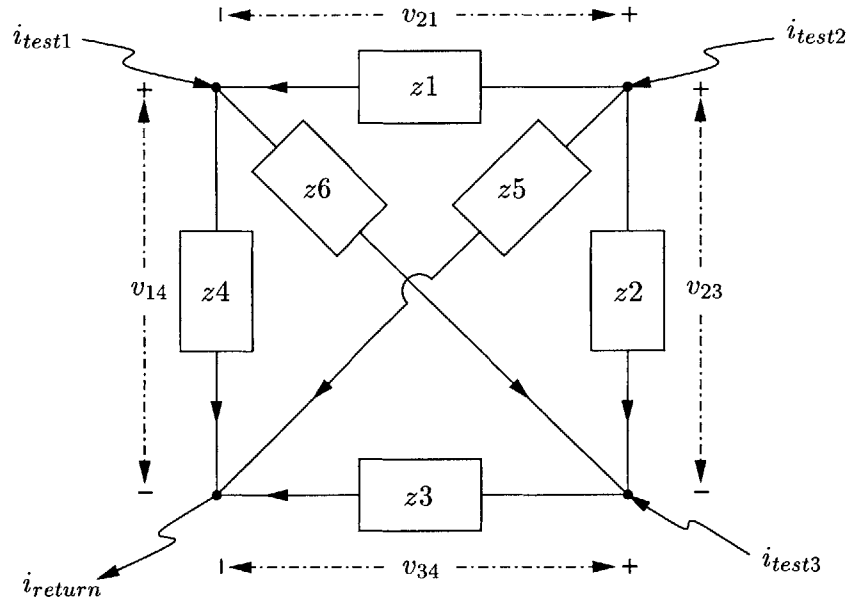
Figure 2-11: A diagram of the voltage and current measurements made as reflected in the refined model of the chassis.

i_{test2}, or i_{test3} be injected at the corresponding node while the voltages v_{14}, v_{12}, v_{23}, and v_{34} are measured. It is apparent that the branch currents can not be directly measured, thus precluding the direct determination of all six branch impedances. One important fact to note from this diagram is that, while the branch currents are not uniquely specified by

30

one experiment, their sum at each node is constrained by Kirchoff's current law. This idea will factor prominently in the method for obtaining the parameters, which is discussed in the next chapter.

Chapter 3

Parameter Estimation

After the examination and analysis which took place in Chapter 2, a set of continuous-time models for the electric utility and the automobile chassis were obtained. Though these models have their own merits, they will not be useful until a set of parameters mapping particular inputs to particular outputs is obtained. In terms of the structure established in Chapter 1, the goal of this chapter is therefore to find the particular values μ_0 for the chosen model $F(\mu)$ that most accurately reproduce the behavior of the physical system under examination.

A number of different methods of parameter identification were tested and compared. There was a marked difference between the methods used on the electric utility and those used on the automobile, however. In order to illustrate this difference, consider the parameter estimation of the system described in Equation 3.1.

$$y(t) = \mu_0 \frac{dx^n}{dt} + \mu_1 \frac{dx^{n-1}}{dt} + \cdots + \mu_{n-1} \frac{dx}{dt} + \mu_n x(t) \tag{3.1}$$

$$= \mu_0 s^n + \mu_1 s^{n-1} + \cdots + \mu_{n-1} s + \mu_n \tag{3.2}$$

Under the assumption (which will be demonstrated shortly) that there exist methods for using only $x(t)$ and $y(t)$ to find values of μ_0 through μ_n that accurately represent the system, it is clear that the problem of estimating the parameters of the electric utility can be solved. Unfortunately, this fact does not imply that the estimation of the automobile chassis is also possible with the same methods. While the individual branches in the model conform to the above input/output relationship, the input variable in the above formulation cannot be directly measured. In order to characterize the automobile chassis, a series of modifications

must therefore be made to the approach taken in estimating the parameters of the electric utility. These changes will be described in detail.

3.1 The Electric Utility

Two different methods were evaluated in the process of performing the parameter identification of the electric utility. The first method, referred to as the λ method, estimates the parameters of the continuous time transfer function (i.e. computes the R and L of the electric utility.) This is useful because it can be checked against physical intuition regarding the expected values of resistance and inductance.

The second method, referred to as the ARMAX method, estimates the parameters of an equivalent discrete-time model. The parameters of this transfer function can be related to the continuous-time parameters via a mapping in the complex plane, such as the bilinear transformation [10]. Though these discrete-time model parameters do not give the same degree of insight as an equivalent set of continuous-time parameters, the sampled data environment where both identification and the prediction of voltage distortion are performed is more conducive to the use of discrete-time models.

3.1.1 The λ Method

Consider the relationship between $i(t)$ and $v(t)$ governed by the following general continuous-time transfer function

$$i(t)\left(R_0 + Lp + \delta p^2\right) = \hat{v}_s(t) - v(t) \tag{3.3}$$

where the time-differentiation operator $p = \frac{d}{dt}$. The process of directly finding the parameters R_0, L, and δ of this system would be possible if the quantities $i(t)$, $pi(t)$, $p^2 i(t)$, and $(\hat{v}_s(t) - v(t))$ were available for measurement. Unfortunately, only the quantities $i(t)$ and $\hat{v}_s(t) - v(t)$ are accessible, so that a method for obtaining $pi(t)$ and $p^2 i(t)$ from $i(t)$ is necessary. The most intuitive way for obtaining the parameters, that of approximating the derivatives with differences, is extremely sensitive to noise and is not a viable solution. As an alternative to measuring or approximating p, introduce the λ operator as given in Equation 3.4.

$$\lambda = \frac{1}{1 + p\tau}, \quad \tau > 0 \tag{3.4}$$

In order to bypass the problems associated with the derivative, an operator substitution can be made. After some simple manipulation,

$$p = \frac{1 - \lambda}{\tau \lambda}.$$ (3.5)

It is important to note that λ is not a scalar, but rather an operator; this is to say that λx is the result of applying the low-pass operator λ to x. One of this λ operator's attractive properties can be seen from Equation 3.4; as it is a low-pass operator, it tends to filter out high-frequency noise which can introduce bias into the parameter estimates.

In order to use the λ operator to estimate the parameters of the continuous-time transfer function, the relation in Equation 3.5 must be exploited so as to eliminate p from the equation. Performing this substitution and multiplying through by $\lambda \tau$, Equation 3.3 becomes

$$\left(\delta \left(1 - 2\lambda + \lambda^2 \right) + \tau L \left(1 - \lambda \right) + \tau^2 \lambda^2 R_0 \right) i(t) = \tau^2 \lambda^2 \left(\hat{v}_s(t) - v(t) \right)$$ (3.6)

This equation is much more computationally attractive, as the only challenge now is to apply the λ operator to $i(t)$ and $v(t)$ so as to generate $\lambda i(t)$, $\lambda^2 i(t)$, and $\lambda^2 v(t)$. Equation 3.6 can be rewritten so as to produce a linear least-squares tableau

$$\left(\begin{array}{ccc} [\lambda^2(\hat{v}_s - v)](t) & [\lambda i](t) & [\lambda^2 i](t) \end{array} \right) \left(\begin{array}{c} \hat{\mu}_1 \\ \hat{\mu}_2 \\ \hat{\mu}_3 \end{array} \right) = i$$ (3.7)

where

$$\hat{\mu}_1 = \frac{\tau^2}{\delta}$$

$$\hat{\mu}_2 = 2 - \frac{\tau L}{\delta}$$

$$\hat{\mu}_3 = \frac{\tau L}{\delta} - \frac{\tau^2 R_0}{\delta} - 1$$

The estimates of the continuous-time parameters R_0, L, and δ can thus be extracted from $\hat{\mu}$ by simple algebra [15]. The quantities i, v, and v_s are column vectors of N samples each, so that the tableau $\left(\begin{array}{ccc} [\lambda^2(\hat{v}_s - v)](t) & [\lambda i](t) & [\lambda^2 i](t) \end{array} \right)$ contains three columns and N rows. This matrix is low-pass, since the λ operator has acted on all of its columns. Additionally,

the estimates $\hat{\mu}$ will be unbiased as long as N is large. A detailed treatment of the noise model for the λ method can be found in [7].

The parameter τ is selected by the user so as to preserve the desired information and minimize measurement noise. For the timescales involved in estimating the parameters of the electric utility, $\tau = 0.002s$ were used, but a relatively wide range of τ is acceptable in practice. Practical experience has shown that the operator, although designed to work in a continuous-time sense, can be applied to finely sampled quantities with little error.

It also is important to note for implementation's sake that the tableau could have instead been formulated as it is in Equation 3.8.

$$\left(\begin{array}{ccc} [i - 2\lambda i + \lambda^2 i](t) & \tau[1 - \lambda i](t) & \tau^2[\lambda^2 i](t) \end{array} \right) \left(\begin{array}{c} \delta \\ L \\ R_0 \end{array} \right) = \tau^2[\lambda^2(\hat{v}_s - v)](t) \qquad (3.8)$$

This formulation was not used because the condition number of the resulting tableau would have been much larger than the condition number of the tableau in Equation 3.7. Since the accuracy of the linear least-squares solution is proportional to the square of the condition number, the estimate generated by the tableau of Equation 3.8 would not have been nearly as accurate as that which was generated by Equation 3.7.

An Example

As a simplified example of how the λ operator substitution method works, consider the circuit in Figure 3-1. The goal of this example is the identification of R_2 and L, where $R_2 = 0.02\Omega$ and $L = 12\mu H$. If the MOSFET is used as a switch, a snapshot of both $i(t)$ and $v(t)$ shortly before and after the MOSFET is turned on are illustrated in Figures 3-2 and 3-3. These simulations were generated with Matlab; the code is available in Appendix C. Note that some random noise was added to each signal in order to simulate the effects of measurement noise.

Many of the problems inherent in the experimental setup of the electric utility have obviously been left out of this example for the sake of simplicity. To continue the example, the model for the system to be modelled is as follows in Equation 3.9.

$$(R + Lp)i(t) = v(t) \qquad (3.9)$$
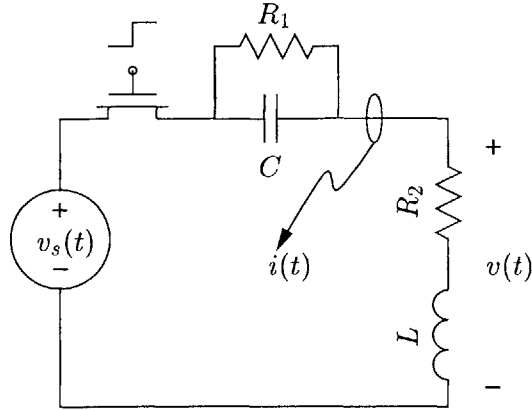
Figure 3-1: Example circuit used to illustrate the mechanics of the λ method.
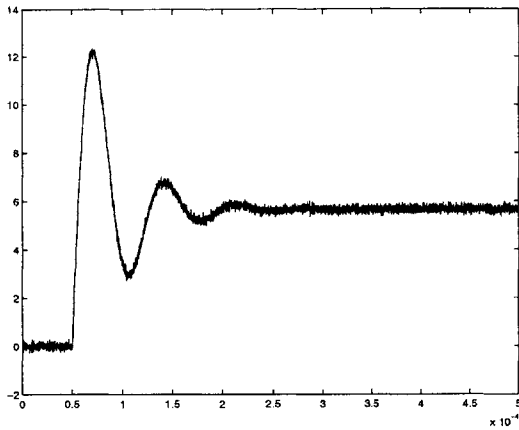
Figure 3-2: Plot of $i(t)$ resulting from a step in $v_s(t)$.
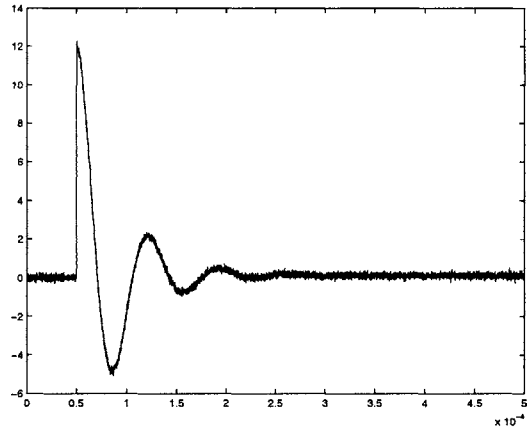
Figure 3-3: Plot of $v(t)$ resulting from a step in $v_s(t)$.

By performing the substitutions suggested by Equation 3.5, the following linear least-squares tableau results.

$$\left(\begin{array}{cc} [\lambda v](t) & [\lambda i](t) \end{array} \right) \left(\begin{array}{c} \frac{\tau}{L} \\ \left(1 - \frac{\tau R}{L}\right) \end{array} \right) = i(t) \qquad (3.10)$$

A τ of $5 \times 10^{-5}s$ is chosen by taking the time scale into account, and the filtered voltages are generated using the lsim command in MATLAB. These voltages are plotted in Figure 3-4.

Notice that one of the beneficial features of the λ method is evident in this plot; the noise which was present in the original voltage and current waveforms has been filtered out. As these waveforms are used as the regressors in the least-squares tableau, the parameters

36
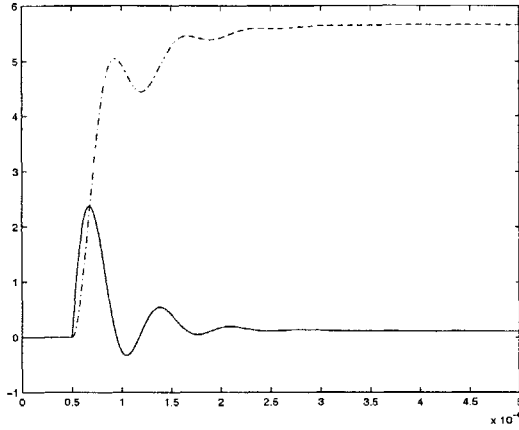
Figure 3-4: Plot of the low-pass filtered current and voltages. λi is dotted, while λv is solid.
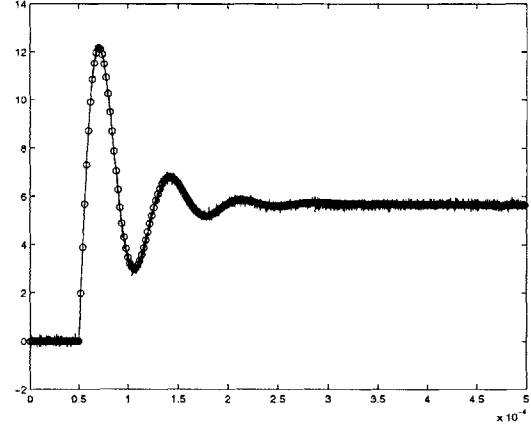
Figure 3-5: Plot illustrating the effectiveness of the λ method. $i(t)$ is solid, while $\hat{i}(t)$ is denoted with points.

that they produce will not show the effects of the noise.

Though it has many desirable properties, the λ method is not entirely without faults. If the waveforms contain a good deal of bias which is corrupting the desired data, such as measurement noise, the parameter estimates will reflect the least-squares fit to this corrupted information. Additionally, if the waveform has a very low amount of frequency content, the parameters will be very sensitive to the value of τ which is chosen. Finally, the filtering property of the λ method is beneficial if the group of frequencies containing noise are segregated from the frequencies of the measurement signal, but if frequencies of the measurement and the noise are close to one another, then the filtering effect of the λ method will eliminate some of the information which would be used to obtain parameter estimates.

In this example, however, neither of these issues is pertinent, as is possible to see from the parameters obtained from the least-squares solution of the tableau. The estimated values of the parameters are $\hat{L} = 12.067\mu H$ and $\hat{R} = 0.0202\Omega$. These parameters are very close to the actual parameters; a plot of the predicted current and the actual current in Figure 3-5 shows high quality of fit.

37

3.1.2 The ARMAX Method

As previously mentioned, one of the principal problems with the λ method is that it is not able to model some types of colored noise, such as DC offsets. In comparison, ARMAX models (autoregressive moving average with exogenous input) include a noise model that can fit colored noise as well as the response of the modelled system.

Recall the continuous-time model in Equation 3.3. By using a mapping from continuous-time to discrete-time, such as the bilinear transformation, a discrete-time approximation to the above model can be obtained. This approximate model can be written

$$P_a^2(z^{-1}) \left(\hat{v}_s[k] - v[k] \right) = P_b^2(z^{-1})i[k], \tag{3.11}$$

where $P_a^n(z^{-1})$ denotes an nth-order polynomial in $z-1$ with coefficients a_k, e.g.

$$P_a^2(z^{-1}) = a_0 + a_1 z^{-1} + a_2 z^{-2} \tag{3.12}$$

The fundamental improvement which the ARMAX model makes over the basic discrete time model is that a colored noise term is added to the transfer function which is being estimated. This allows the model to accommodate colored noise which would otherwise bias the parameters. Equation 3.13 shows the discrete-time model for the electric utility with the colored noise term, which was fit using the ARMAX routine available in the MATLAB System Identification toolbox.

$$P_a^2(z^{-1})(\hat{v}_s[k] - v[k]) = P_b^2(z^{-1})i[k] + P_c^4(z^{-1})e[k] \tag{3.13}$$

3.2 The Automobile Chassis

As was the case with the electric utility, the parameter estimation of the automobile chassis was investigated in both a continuous-time and a discrete-time sense. The continuous-time λ method was again used to obtain the parameters; unfortunately, it did not work very well. Some of the fundamental problems present in using the λ method to identify the parameters of the model of the chassis as contained in Figure 2-10 will be discussed in the following sections.

Additionally, this section will also present a discrete-time model which was also tested.

This discrete-time model was derived from the continuous-time model in a slightly different way than the discrete-time model of the electric utility. Furthermore, the limitations placed on the parameter estimation of the model required that a specialized method be implemented, rather than a cookbook approach taken by a routine like ARMAX. This method will also be explained.

As will become clear shortly, it is generally more difficult to estimate the parameters of a 12-element model than a 2-element model. In a general sense, the engineer attempting to obtain parameter estimates might not recognize this fact, as the existence of codes such as are contained in the System Identification toolbox of MATLAB do most of the work without providing much of a hint as to their workings. In this case, the specificity of both the continous-time and discrete-time models prohibit the use of such programs. As linear least-squares techniques cannot be used to minimize $(y - \hat{y})$ for either model of the chassis, an abbreviated explanation of a method for performing nonlinear minimization is given in the following section.

3.2.1 Nonlinear Minimization

As stated in the introduction of this chapter, the goal of parameter estimation is to find some set of values $\hat{\mu}$ which will make the predicted output $f(x, \hat{\mu}) = \hat{y}$ as close as possible to the actual output y. Though there are many different ways of measuring the degree of "closeness," one common standard is making the sum of the squared differences between the two functions as small as possible. Cast in the context of parameter identification, this means that the goal is finding some optimal value of $\hat{\mu}$ which will minimize the function $g(\hat{\mu})$, where g is defined by

$$g(\mu) = y - f(x; \mu) \tag{3.14}$$

This step is performed most easily when the system is linear, so that $f(x, \hat{\mu})$ can be expressed as a matrix multiplication $A\hat{\mu}$. One of the reasons that the λ is so attractive, in fact, is that it can be formulated as a linear least squares problem. In this case, the minimum sum of the squared differences between $A\hat{\mu} = \hat{y}$ and y can be calculated analytically, as given in Equation 3.15.

$$\hat{\mu} = \left(A^T A\right)^{-1} A^T b \tag{3.15}$$

Unfortunately, the situation often arises where the loss function $g(\mu)$ consists of a set of nonlinear equations. The loss functions which arise in the identification of the model parameters of the automobile chassis fall into this category. It is therefore necessary to resort to numerical methods, whereby an initial guess for the parameters $\hat{\mu}$ is proposed and then refined via an iterative algorithm.

If one were to ponder the problem of finding the minimum of some n-dimensional surface with any number of curves and valleys, a number of geometric strategies would probably leap to mind. One strategy might be to start at some initial point, look for the direction in which the surface moved most rapidly downward, and then pick the next point so as to move in that direction. Another strategy might be to pretend that the whole surface was governed by the behavior around that initial point, linearize around that point, and then pick the next point so as to place it at the minimum of that linearized surface. These two strategies constitute the essence of two popular minimization methods: steepest descent and Gauss-Newton. Though treatments of both of these algorithms are fascinating, extensive analyses have already been written and are beyond the scope of this thesis; for the purposes of sufficient background, each method is summarized below.

The steepest descent method of minimization is a fairly simplistic one, as it looks in the direction of the steepest downward slope to pick the next point. In other words, the minimization proceeds along the negative gradient at each iteration so that the step δ_g required to compute $\hat{\mu}_{k+1} = \hat{\mu}_k + \delta_g$ is given by

$$\delta_g = -\alpha \left(\frac{\partial g}{\partial \mu_1}, \frac{\partial g}{\partial \mu_2}, \cdots, \frac{\partial g}{\partial \mu_n} \right) \Bigg|_{\hat{\mu}_k} \qquad (3.16)$$

where α is chosen so that the minimization proceeds along the negative gradient. A thorough exposition of the steepest gradient method is given in [14].

By way of comparison, the Gauss-Newton minimization algorithm is fundamentally as straightforward as the steepest descent method. The mathematical notation is more difficult to follow, unfortunately. The method constructs the first order Taylor expansion of the nonlinear function around the starting point $\hat{\mu}_k$ so that the linearized set of equations adopt a familiar form, as seen below.

$$J\delta_l = b \qquad (3.17)$$

where δ_l is the step that takes $\hat{\mu}_k$ to $\hat{\mu}_{k+1}$, J is the jacobian evaluated at $\hat{\mu}_k$, and b is a

combination of y, $\hat{y}$, and $f(x;\mu)$ evaluated at $\hat{\mu}_k$. The form of the solution to this linearized set of equations is therefore given by Equation 3.15, which produces the value of δ_l needed to reach the new linearized minimum from $\hat{\mu}_k$. A formal treatment of the Gauss-Newton approach to minimization is given in [3].

Unfortunately, many of the minimization problems encountered in experimental circumstances bring out the shortcomings of these methods. Two such problems that arise while using the Gauss-Newton method occur with loss functions that possess local minima as well as a global minimum. The first problem arises because the direction in which the minimization proceeds at each step assumes that the linearization is valid over the entire parameter space. This is obviously false, as evident by the presence of many local minima. Furthermore, the Gauss-Newton method is prone to getting stuck in local minima, rather than finding the global minimum. Both of these problems can be manifest when considering good and bad initial guesses; with a bad initial guess, Gauss-Newton can easily get stuck in a local minimum. With an initial guess reasonably close to the global minimum, on the other hand, Gauss-Newton might assume that the linearization holds over a larger region than it actually does. This can result in a step which overshoots the global minimum, thereby putting the method once again at risk of converging on a local minimum.

Though the method of steepest descent is not as prone to getting caught in local minima, it has its own particular problem: it tends to converge very slowly. If the loss function is a narrow valley, the steepest descent solution will bounce back and forth across the valley, zeroing in on the global minimum at a very gradual rate. This convergence happens so gradually, in fact, that the amount of time required to find the minimum is often prohibitively large.

The Levenberg-Marquardt algorithm was devised with the hope of creating an algorithm which uses some of the traits of both the Gauss-Newton method and the steepest descent method. The Levenberg-Marquardt algorithm generally behaves much like the Gauss-Newton method, but it enforces a step size limit because it acknowledges the fact that the linearization of Gauss-Newton is not valid over the entire parameter space. By enforcing the limit in step size, the Levenberg-Marquardt method can approach the direction in which steepest descent would converge. Levenberg-Marquardt is still somewhat susceptible to the perils of local minima, but it is less so than Gauss-Newton. The ability of this algorithm to quickly and reliably find the value of $\hat{\mu}$ at which a loss function was minimized

was used extensively in estimating the model parameters of the automobile chassis, as will be demonstrated in the following sections.

3.2.2 The λ Method Revisited

As illustrated by the example of the electric utility, the λ method works by directly estimating the numerator and denominator coefficients of a transfer function. One quality of the transfer function model of the utility that made this method so successful, however, was the fact that each coefficient was only related to one system parameter. Stated differently, the effectiveness of the λ method was partially due to the fact that the highest power of s was only related to the inductance L, while the coefficient of the constant term was only related to the DC resistance R_0. The significance of this fact becomes evident when attempting to use the λ method to find the parameters of the automobile chassis. Recalling the experimental setup for collecting parameter estimation data (as shown in Figure 3-6) it is clear

i_{test1} v_{21} i_{test2}

$z1$ $z6$ $z5$ v_{14} $z4$ $z2$ v_{23} $z3$ v_{34} i_{test3} i_{return}
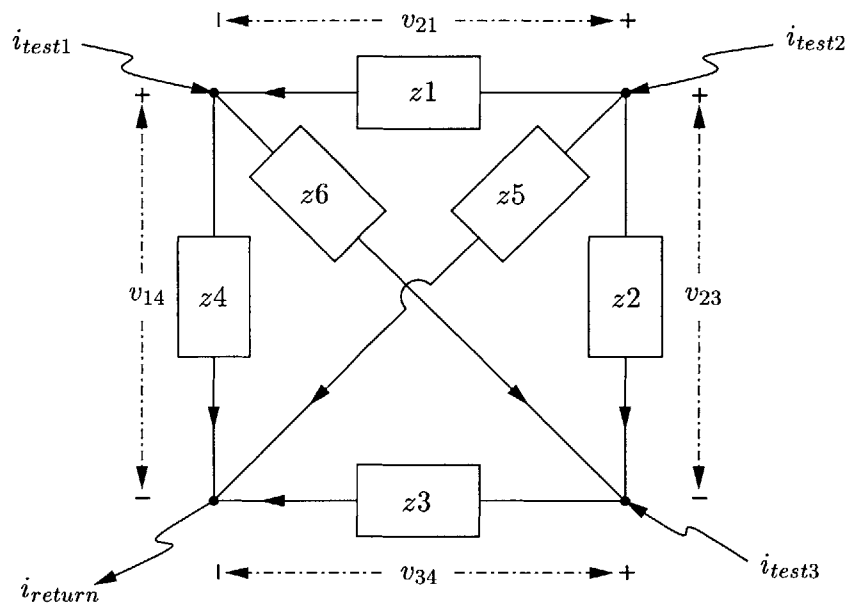
Figure 3-6: A diagram of the voltage and current measurements made as reflected in the refined model of the chassis.

that the transfer functions relating the voltage across any branch to the total current flowing into the network will be very complicated. These transfer functions were calculated by entering the loop and node equations into MAPLE, and solving for the analogous transfer functions from current into nodes 1, 2, and 3 to the four voltages v_{14}, v_{21}, v_{23}, v_{34}. These

transfer functions are tabulated in Appendix B; suffice it to say that even a short glance at them will reveal their extremely nonlinear qualities.
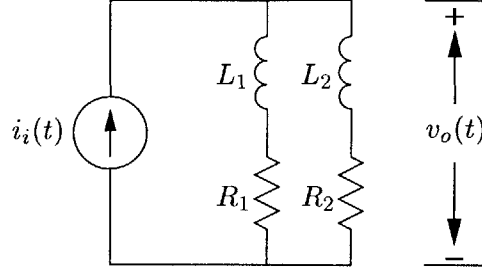
Figure 3-7: Example circuit illustrating a transfer function which is nonlinear in the continuous-time parameters.

An example illustrating a transfer function which has nonlinearities in its component parameters is given by the circuit in Figure 3-7. Consider the following transfer function from $i_i(t)$ to $v_o(t)$:

$$\frac{v_o}{i_i} = \frac{L_1 L_2 s^2 + (L_1 R_2 + L_2 R_1)s + R_1 R_2}{(L_1 + L_2)s + (R_1 + R_2)} \tag{3.18}$$

Additionally, the λ linear least-squares tableau resulting from this transfer function is given by Equation 3.19.

$$\left(\begin{array}{cccc} [\lambda^2 v_o](t) & [\lambda v_o](t) & [\lambda^2 i_i](t) & [\lambda i_i](t) \end{array} \right) \left(\begin{array}{c} \hat{\mu}_1 \\ \hat{\mu}_2 \\ \hat{\mu}_3 \\ \hat{\mu}_4 \end{array} \right) = i_i \tag{3.19}$$

where

$$\hat{\mu}_1 = \frac{\tau^2(R_1 + R_2) - \tau(L_1 + L_2)}{L_1 L_2} \tag{3.20}$$

$$\hat{\mu}_2 = \frac{\tau(L_1 + L_2)}{L_1 L_2} \tag{3.21}$$

$$\hat{\mu}_3 = \frac{\tau(L_1 R_2 + L_2 R_1) - L_1 L_2 - \tau^2 R_1 R_2}{L_1 L_2} \tag{3.22}$$

$$\hat{\mu}_4 = \frac{2L_1 L_2 - \tau(L_1 R_2 + L_2 R_1)}{L_1 L_2} \tag{3.23}$$

The nonlinear relationships between the component values (i.e. R_k and L_k) show that

the values of R_1, R_2, L_1, and L_2 are not immediately obtainable from the results of the λ method in the same manner as the continuous-time parameters of the electric utility were obtained (Equation 3.7). It is also important to mention the fact that the above example is fairly simple; the parameters of the transfer functions of the automobile chassis as produced by the λ method are much more complicated.

As illustrated by the previous example, the use of the λ method in directly estimating the resistances and inductance of the chassis model is experimentally untenable. The set of intermediate parameters obtained via the λ method is related to the desired component values, however; by using a nonlinear minimization routine, a set of component values can be found which are related to the intermediate values.

With this knowledge, a strategy may be devised for obtaining the parameters of the automobile chasssis for the continuous-time model via the λ method. The first step is the solution for the intermediate parameters of all of the transfer functions via the λ method. This step proceeds along exactly the same lines as the solution for the parameters of the electric utility and produces twelve sets of parameters, each of which describes a transfer function from one of the test currents to one of the measured branch voltages. These sets of parameters are then entered into a nonlinear equation solver, such as one using nonlinear least-squres techniques, to derive the parameters of the continuous-time model.

3.2.3 Discrete-Time Identification

As has been mentioned earlier in this chapter, the additional complexity built into the model of the automobile chassis is the cause of a number of differences between the process of parameter estimation for the electric utility and the automobile chassis. It has been shown that the continuous-time parameter identification of the utility differs from the chassis in many respects; this difference is also manifest in the model of the discrete-time models of the two systems. The first aspect in which these two models are different involves the manner in which the discrete-time model is constructed from the continuous-time model.

Recall that the model of the automobile chassis is constructed in such a way as to resemble the interconnection of six steel plates between four nodes, where each of the steel plates is modelled as the series connection of an inductor and a resistor. Rather than use sophisticated methods to convert the continuous-time model into a discrete-time model, a simple first-order difference method was used to motivate the discrete-time model of the

steel plate. According to this method, also known as the Euler method [11], the following expression serves as an approximation to the derivative of a function $f(x)$:

$$f'(x) \simeq \frac{x[k] - x[k-1]}{h} \tag{3.24}$$

where h is the step size, or the distance between consecutive samples. Given the ability to approximate derivatives, it is clear that a simple discrete-time model can be formulated, as demonstrated below.

$$v(t) = Ri(t) + L\frac{di}{dt} \tag{3.25}$$

$$v(t) \simeq v[k] \tag{3.26}$$

$$v[k] = Ri[k] + L\left(\frac{i[k] - i[k-1]}{h}\right) \tag{3.27}$$

$$v[k] = \mathbf{a}i[k] + \mathbf{b}i[k-1] \tag{3.28}$$

The discrete-time model therefore looks much like the continuous-time model, the only difference being that each branch possesses the terminal relationship expressed in Equation 3.28 rather than that of Equation 3.25. It is significant that this discrete-time model has nothing to do with numerical integration, a task for which the Euler method is normally used. The Euler method is merely mentioned as a motivation for approximating the continuous-time model with a discrete-time formulation.

Now that a discrete-time model of the automobile chassis has been identified, it is necessary to explain the method by which the parameters of the model are obtained. This method can be divided into two distinct layers. Recalling that the end goal of this thesis was the prediction of voltage distortion at a set of points on the car, it is therefore logical to construct the top layer of the parameter estimation so that its objective consists of minimizing a loss function $g(\mu) = v[k] - \hat{v}[k]$ over all datapoints k. By adjusting $\hat{\mu}$ so as to minimize the differences between the actual voltages and predicted voltages over a wide range of test current inputs, the set of $\hat{\mu}$ will be able to predict the voltage distortion at the prescribed set of points as well as possible.

The second layer of the parameter identification is somewhat more subtle, as it involves generating a set of $\hat{v}$ from a given set of μ so that $g(\mu)$ can be evaluated and minimized. This could obviously be accomplished if the currents through each branch were known;

as the discrete-time model under study is only an approximation of a continuous system, however, the measurement of these "currents" could never actually take place.

Given that the measurement these individuals currents is not an option, consider instead the relationship of the measurable current (i_{test}) to the currents in the individual branches. Though the branches of impedances in the car are an approximation, the voltage across and current through each of the branches still need to obey Kirchoff's laws. This fact permits the construction of a number of constraints on the terminal variables. With the currents and voltages being constrained by KCL and KVL, as well as the test current, the individual branch currents can be solved for in a least-squared sense. The branch voltages can be determined from these branch currents, and the nonlinear least-squares routine can thereby calculate successive values of $g(\mu)$ as the minimization converges upon the optimal value of $\hat{\mu}$.

Though the above description effectively outlines the manner in which the parameters of the discrete-time model are estimated, the process is understood much more easily via an example, as given below.

An Example

Referring to Figure 3-6, consider the experiment in which the test current is injected into node 2. By simply summing up the currents flowing into nodes 1, 2, and 3 and writing three independent voltage loops, the following constraints can be written:

$$0 = i_4[k] + i_6[k] - i_1[k] \tag{3.29}$$

$$i_{test2}[k] = i_1[k] + i_2[k] + i_5[k] \tag{3.30}$$

$$0 = i_3[k] + i_6[k] - i_2[k] \tag{3.31}$$

$$0 = v_1[k] + v_4[k] - v_5[k] \tag{3.32}$$

$$0 = v_3[k] - v_4[k] + v_6[k] \tag{3.33}$$

$$0 = v_2[k] - v_1[k] - v_6[k] \tag{3.34}$$

In order to use these constraints in solving for the currents in a linear least-squares fashion, Equations 3.29 through 3.34 must be written in matrix notation. The KCL equations are

46

most easily reformulated, as is done below:

$$\begin{pmatrix} -1 & 0 & 0 & 1 & 0 & 1 \\ 1 & 1 & 0 & 0 & 1 & 0 \\ 0 & -1 & 1 & 0 & 0 & 1 \end{pmatrix} \begin{pmatrix} i_1 \\ i_2 \\ i_3 \\ i_4 \\ i_5 \\ i_6 \end{pmatrix}_{[k]} = \begin{pmatrix} 0 \\ i_{test} \\ 0 \end{pmatrix}_{[k]} \qquad (3.35)$$

$$\mathbf{A}\mathbf{i}[\mathbf{k}] = \mathbf{b}[\mathbf{k}] \qquad (3.36)$$

where the subscript $[k]$ denotes that the relation holds for the kth sample and the abbreviations made in Equation 3.36 are for the purposes of later notational simplicity. One notable fact is that more constraints are necessary for the successful solution of the problem, as there are effectively still three free variables.

In order to include additional constraints, the KVL constraints must be translated into relations between the currents. By taking advantage of the model for the individual branches (Equation 3.28), the following constraints can also be written as:

$$\mathbf{P_a}\mathbf{i}[\mathbf{k}] + \mathbf{P_b}\mathbf{i}[\mathbf{k} - 1] = \mathbf{0_v} \qquad (3.37)$$

where

$$\mathbf{P_a} = \begin{pmatrix} a_1 & 0 & 0 & a_4 & -a_5 & 0 \\ 0 & 0 & a_3 & -a_4 & 0 & a_6 \\ -a_1 & a_2 & 0 & 0 & 0 & -a_6 \end{pmatrix} \qquad (3.38)$$

$$\mathbf{P_b} = \begin{pmatrix} b_1 & 0 & 0 & b_4 & -b_5 & 0 \\ 0 & 0 & b_3 & -b_4 & 0 & b_6 \\ -b_1 & b_2 & 0 & 0 & 0 & -b_6 \end{pmatrix} \qquad (3.39)$$

and the $\mathbf{0_v}$ is of the required dimension.

By subtracting the $(k-1)$th currents from both sides of the equation, the KVL and KCL

47

constraints can be combined to form one linear set of equations, as given in Equation 3.40.

$$
\begin{pmatrix} \mathbf{A} \\ \mathbf{P_a} \end{pmatrix} \mathbf{i[k]} = \begin{pmatrix} \mathbf{b[k]} \\ \mathbf{0_v} \end{pmatrix} - \begin{pmatrix} \mathbf{0_M} \\ \mathbf{P_b} \end{pmatrix} \mathbf{i[k-1]}
\tag{3.40}
$$

where the $\mathbf{0_M}$ matrix is again of the required dimension.

This is recognizable as a linear system of equations $Ax = b$, which may be iteratively solved in a least-squared sense for $\mathbf{i[k]}$ for every k from $k = 1$ to $k = N$, where there are N datapoints. The initial currents $\mathbf{i[k = 0]}$ must be supplied by the user, but this condition is easily accommodated by making sure that no current is flowing through the car at the beginning of the characterization experiment.

Now that the individual currents flowing through the six branches have been computed, the predicted voltages must be computed so that the residual $g(\mu) = v - \hat{v}(\mu)$ can be generated and minimized. This is accomplished by applying Equation 3.28 in a straightforward manner; the following iterative equation is used as k varies from 1 to N to generate $\hat{v}$.

$$
\begin{pmatrix} v_1 \\ v_2 \\ v_3 \\ v_4 \end{pmatrix}_{[k]} = \begin{pmatrix} \mathbf{a_1} & 0 & 0 & 0 \\ 0 & \mathbf{a_2} & 0 & 0 \\ 0 & 0 & \mathbf{a_3} & 0 \\ 0 & 0 & 0 & \mathbf{a_4} \end{pmatrix} \begin{pmatrix} i_1 \\ i_2 \\ i_3 \\ i_4 \end{pmatrix}_{[k]} + \begin{pmatrix} \mathbf{b_1} & 0 & 0 & 0 \\ 0 & \mathbf{b_2} & 0 & 0 \\ 0 & 0 & \mathbf{b_3} & 0 \\ 0 & 0 & 0 & \mathbf{b_4} \end{pmatrix} \begin{pmatrix} i_1 \\ i_2 \\ i_3 \\ i_4 \end{pmatrix}_{[k-1]}
\tag{3.41}
$$

As stated earlier, these voltages $\hat{v}$ are then used to construct the residual $g(\mu)$ which is minimized via nonlinear least squares; the output of the iterative minimization is the value of μ which most closely describes the behavior of the real system.

Two points bear further comment with regard to the above method of discrete-time identification. The first of these comments has been implied during this discussion, but its importance requires that it be made explicit. Any one experiment will produce a model which captures the parameters well as they relate the current flowing in one node to the voltage distortion at all points on the car. This model will not be able to predict the voltage distortion due to a current injected at another of the nodes, however. In order to produce the best overall estimates of the parameters, a set of experiments must be run, in each of which a current is injected into one of the possible nodes and the set of voltage waveforms recorded. By minimizing all of the residuals from a group of experiments at one time, the

estimate of parameters will reflect the best general estimate of the voltage distortion which can be produced.

The second comment regards the sample rate of the model. It is crucial that the characterization data and the data for simulation be sampled at the same rate; the importance of this fact can be seen by looking at the poor prediction shown in Figure 3-8. The discrete-
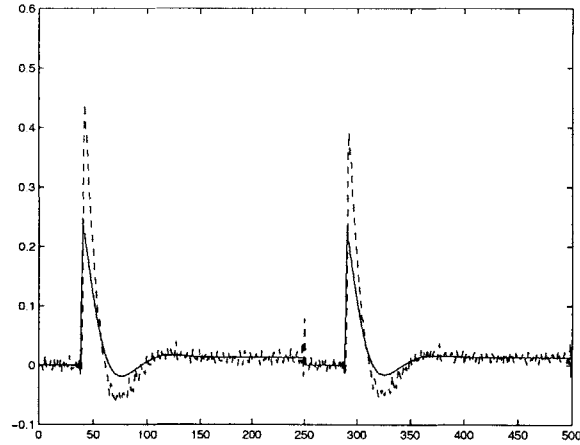
Figure 3-8: Poor voltage prediction waveforms. The solid line is the concatenation of the two measured voltages v_{34} and v_{14}, while the dotted line is the discrete-time prediction of these same two voltages.

time identification process identified a model with a set of data which had a sampling period of $T = 1\mu s$. This model was used in attempt to predict the voltages of a current waveform identical to the one used for identification except for the sampling period, which was changed to $T = 2\mu s$. This demonstrates the need to acknowledge the sampling rate of the model characterization data when using the model to run simulations. In practice, models which were obtained using characterization data over a wide range of sampling rates were found to be successful, as long as the cross-validation data was sampled at the correct rate. An example is given below for the purposes of illustrating the dependence of the model on the sampling rate of the characterization data, as well as a means for accommodating differences between the sampling rates of the characterization data and simulation input data.

Suppose that there exists some voltage and current characterization data with a sampling period T_s which obey the relations $v[k] = v(kT_s)$ and $i[k] = i(kT_s)$, and that there is a

49

discrete-time model (Equation 3.42) which relates the two variables.

$$v[k] = \mathsf{a}i[k] + \mathsf{b}i[k-1] \qquad (3.42)$$

If some new characterization data is taken at a new sampling rate $\hat{T}_s = 10T_s$ and there is a different model which relate the new sampled voltage $\hat{v}[k] = v(k\hat{T}_s)$ and current $\hat{i}[k] = i(k\hat{T}_s)$, then it is possible to express the parameters of the new model in terms of the data taken at the original sampling rate T_s.

$$
\begin{aligned}
\hat{v}[k] &= \hat{\mathsf{a}}\hat{i}[k] + \hat{\mathsf{b}}\hat{i}[k-1] & (3.43) \\
\hat{v}[k] &= v(k\hat{T}_s) & (3.44) \\
v(k\hat{T}_s) &= \hat{\mathsf{a}}i(k\hat{T}_s) + \hat{\mathsf{b}}i((k-1)\hat{T}_s) & (3.45) \\
v(10kT_s) &= \hat{\mathsf{a}}i(10kT_s) + \hat{\mathsf{b}}i(10(k-1)T_s) & (3.46) \\
v[10k] &= \hat{\mathsf{a}}i[10k] + \hat{\mathsf{b}}i[10(k-1)] & (3.47)
\end{aligned}
$$

This shows that the model $(\hat{\mathsf{a}}, \hat{\mathsf{b}})$ can be used at a different sample rate than $\hat{T}_s$, but that the difference in sample rates must be accounted for.

The rate at which the samples are taken is also an essential element in the implementation of the parameter estimation process. A more intuitive way in which to understand the dependence is that the waveforms will change less between samples as the sampling rate increases, thereby making the columns of the matrix containing the data nearly identical and causing difficulties in the process of parameter estimation. The differences between the columns in the data matrix will also be affected by the the finite precision of the computer.

Chapter 4

Experimental Validation

Up to this point in the thesis, models and parameter estimation methods have been developed on a mostly theoretical basis. The primary goal of this chapter therefore consists of presenting the experimental techniques required to perform system identification and cross-validation for the electric utility and the automobile. Furthermore, the experimental results obtained by applying these techniques will be given.

In order to obtain the data required to successfully identify the model parameters, it was necessary to prepare a characterization experiment. In the cases of both the electric utility and the automobile chassis, this setup involved both the construction of specialized hardware to excite the system as well as the specification of a method for measuring the resulting current and voltage waveforms. A set of hardware built explicitly for the purpose of system identification was needed so that the the effects of all modelled parameters were manifest in the data. This can be seen easily by considering the case of the electric utility. Given that the model of the utility consists of $H(s) = R_0 + Ls + \delta s^2$, estimating the parameters L and δ would be impossible unless the characterization waveforms exhibited some time-varying behavior.

Although transient-excitation hardware is essential, the overall success of the experiment is equally dependent upon a detailed and well-conceived data-collection framework. The importance which should be placed on the data-collection setup can be justified in two ways. First, unfortunate choices in measurement can often introduce errors which are otherwise avoidable. For example, an inadvisable method for measuring a resistance on the order of $\sim 0.01\Omega$ would involve making two measurements. The first would measure

52

the v/i relationship 1K resistor alone, while the second would measure the v/i relationship of a 1K resistor in series with the unknown resistance. The unknown resistance could then be theoretically determined from the difference between the two measurements; this method would not be recommended because the two measurements would make it much more susceptible to noise. A better method would involve making a direct measurement of the resistance (assuming this is possible).

The second reason for emphasizing a carefully designed measurement process is the fact that the identification will choose parameters for the model in such a way that the model will fit all available data, including noise, as best as possible. If the noise in the experiment changes dramatically between characterization and simulation in such a way that the measured system changes, the resulting simulation will not correctly represent the behavior of the measured system. Consider the measurement process as illustrated by Figure 4-1.
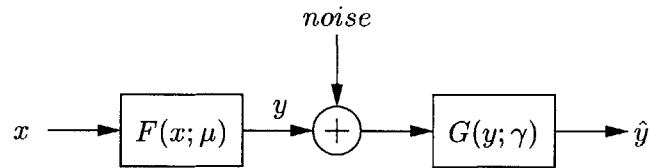
Figure 4-1: General representation of the measurement process, x represents the input, y represents the output of the physical process, and $\hat{y}$ represents the output of the measurement system.

The above diagram illustrates one realistic view of the measurement process, with F representing the system to be identified and G representing the effect that the measurement system has on the actual output. Assume that the system produces a set of outputs $\hat{y}_0$ to the set of characterization inputs x_0, and that the parameter identification routine chooses some set of parameters $\hat{\mu}$ which corresponds to the satisfaction of criteria relating $\hat{y}_0$ and x_0 to the model $\hat{F}$. Note that the behavior of both F and G is captured in the parameters $\hat{\mu}$ of the model. If this model is then used to predict the output $\hat{y}_1$ to some input x_1, the quality of prediction will be similar to the quality of model fit. On the other hand, any change in the measurement system will effectively change G, rendering inaccurate all predictions that $\hat{F}(\hat{\mu})$ could make of $\hat{y}_1$.

Lastly, it is important to review the larger picture of system identification and cross-

validation in the context of this chapter. Both systems are broken down into two sections: a data collection and preprocessing section, and a results section. The data collection portion of each analysis discusses the details of the experimental setup required to generate data from which it is possible to estimate the parameters of the models obtained in Chapter 2. In comparison, the results section is concerned with the degree to which the models actually represent the physical system. The characterization data itself is not presented in the results section, for it is only useful to the extent that it can allow the parameter estimation methods to identify the parameters of the models. The quality of the characterization data is therefore evident only in the ability of the model to predict the actual behavior of the system being studied; it is these data that are presented.

4.1   The Electric Utility

One of the challenges in collecting data for the construction of a model of the utility is that the model must govern the system over a wide range of frequencies. A test setup designed for the purpose of drawing currents is presented, and some of the experimental concerns encountered during construction and measurement of the utility voltage are explained. Finally, a set of results obtained by using the test setup and the techniques discussed in this thesis are given.

4.1.1   Data Collection and Preprocessing

As mentioned in the introduction of this chapter, the ability to obtain parameter estimates from data is strongly dependent upon the effects of the model being manifest. The currents drawn from the wall must therefore cause the wall voltage to distort and sag somewhat. One method for performing this task, as described in [9] and [2], involves connecting a capacitor between line and neutral in the electric utility. The damped oscillations in current and voltage that result from this connection are easily measured and highly repeatable, and thus are useful in obtaining parameter estimates. This thesis takes a somewhat more direct approach to the introduction of voltage distortion; a programmable current source was constructed so that currents could be drawn which created voltage distortion possessing desirable characteristics. These characteristics include the ease of measurability as well as well-defined time and frequency support. A simplified schematic for this current source is

displayed in Figure 4-2.
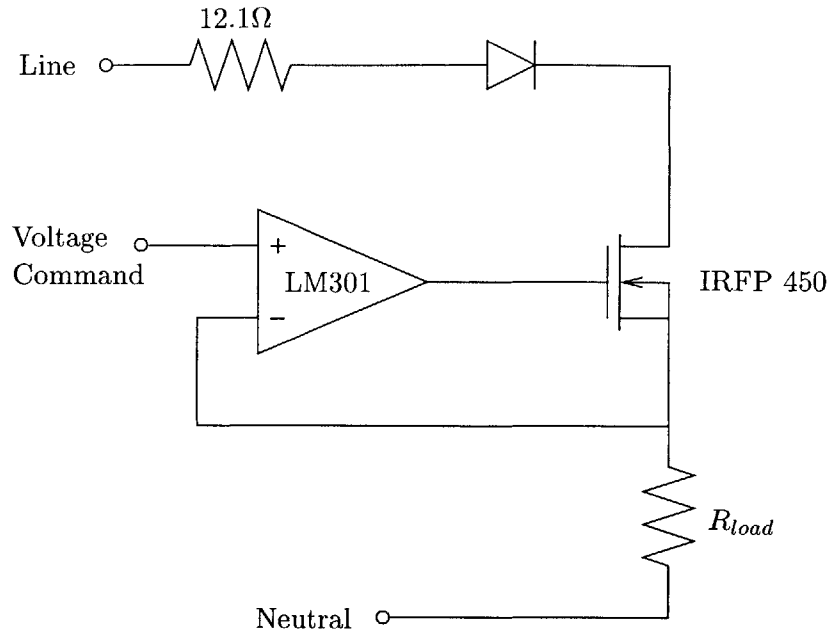
Figure 4-2: Simplified schematic diagram for the current source used to excite transients on the electric utility.

The manner in which this current source works is fairly straightforward. As the op-amp driving the MOSFET is hooked up in a unity-gain follower configuration, the output will attempt to drive the source so that the voltage at its inverting input is identical to the voltage at its non-inverting input. This effectively constrains the voltage at the source of the MOSFET to be identical to the voltage command waveform at the non-inverting input of the op-amp. As the maximum voltage at the source of the MOSFET is equal to the maximum value attained by the voltage command waveform, R_{load} is calculated via Ohm's law so as to yield a peak current I_{peak} which produces the desired amount of voltage distortion. In other words,

$$R_{load} = \frac{V_{peak,command}}{I_{peak,desired}} \tag{4.1}$$

Given that the preliminary design of the current source has been specified, it is necessary to formulate a set of current waveforms which will create the desired amount of voltage distortion. Additionally, the utility must be characterized over a wide range of frequencies in order to produce a valid model. To meet both of these criteria, a set of windowed sinusoids

55

was produced which spanned the frequency range under study. One representative of this set of waveforms is displayed in Figure 4-3. This waveform was synthesized by applying a
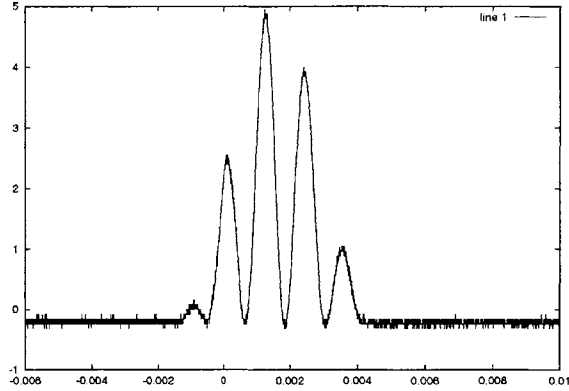
Figure 4-3: Current waveform used to excite voltage distortion on the electric utility.

Hanning window [10] to each of a set of 10 sinusoids ranging in frequency from 65Hz to 900Hz. The series of samples generated by this process is given by

$$i_t[k] = Aw_H[k](1 + \sin(kT_s\omega_t))a \tag{4.2}$$

where w_H is the Hanning window, T_s is the sampling period, ω_t is the frequency of the particular test sinusoid, and A is the amplitude of the test signal. The parameters of this waveform ω_t and w_H were chosen by the frequency of the waveform, T_s was picked so that it was greater than the number of points being sampled by the data acquisition system, and A was chosen so that the peak current drawn from the wall is large enough to cause a measurable amount of voltage distortion.

A few practical issues arose in implementing the current source described above, due to the fact that the a MOSFET was used to command the current waveform. Two well-known properties of MOSFETs are that current can only pass through them in one direction, and that they are designed with certain power dissipation limits. Both of these conditions presented design challenges; since the electric utility generates an AC voltage, the line voltage spends part of its cycle both above and below the neutral voltage. As current cannot flow through a MOSFET in both directions, the device had to be protected from these negative currents. Furthermore, the amplitude of the current required to produce a

56

noticeable voltage distortion on the utility was often near 15A, so the mosfet had to be chosen and protected so that it could withstand a peak power on the order of 1000VA.

These issues were resolved through a variety of steps. To avoid bidirectional current flow, a diode was placed between the line and the drain of the MOSFET. This diode prevented current from flowing whenever the line voltage dropped below the voltage at the source of the MOSFET. The power dissipation issue, on the other hand, was resolved via two steps. First, a 12.1Ω resistor was placed in series with the diode; whenever current was flowing through the test circuit, this resistor would dissipate a portion of the power. Furthermore, the current source was only operated for a few seconds at a time, allowing the time-average power to remain low even though the peak power was relatively high.

One additional problem surfaced with regards to the voltage command for the current source. In examining Figure 4-2, it is notable that the entire circuit, including the op-amp, is referenced to the neutral potential of the utility. Since this potential is not equal to ground, referencing the voltage at the non-inverting terminal of the op-amp with respect to ground will cause a much different voltage command waveform than is intended. In some circumstances, it might be possible to configure the voltage command device so that it too was referenced to neutral. In this case, however, the complexity of the drive waveform required that a Tektronix AWG 2005 arbitrary generator be used to generate the required signals. Since this instrument could not be referenced to neutral, an Analog Devices AD215 isolation amplifier was used to isolate the ground-referenced waveform produced by the AWG 2005 from the drive at the neutral-referenced input to the current source. The AD215 isolation amplifier was chosen because its high ($\sim$ 100kHz) bandwidth enabled it to reproduce the frequency content of the drive signals accurately.

Upon testing the experimental version of the previously described current source, one additional difficulty in measuring the voltage waveform was encountered. Previous experience in using the Tektronix TDS450 oscilloscope to record data had not indicated that there was any significant problem with quantization, but close examination of the data produced by recording a ±168V sine wave showed that the waveform was quantized into approximately 3V steps. Since the amount of voltage distortion due to a 15A current is approximately the same size as the quantization level, it was impossible to estimate the parameters of the distortion because of the low signal-to-quantization noise ratio.

The methods ultimately employed to measure the voltage distortion took advantage of

the fact that the distortion was present on top of the 60Hz power line voltage. The first technique used a differential amplifier to measure the difference between the line and neutral potentials. This had two beneficial effects: it brought the waveform from the distribution voltage to $\pm 3V$, and it referenced the measured signal to ground rather than to neutral. This step eliminated the quantization issue; unfortunately, the relative size of the 60Hz component made the the voltage distortion still difficult to measure.
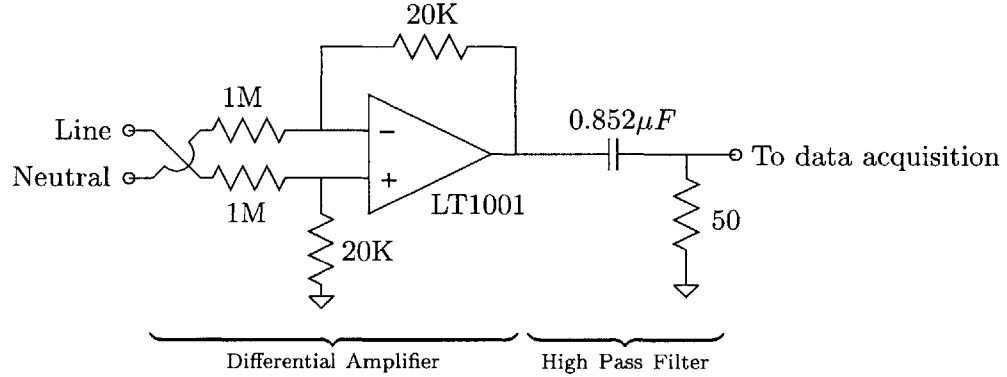
Figure 4-4: Schematic diagram of the circuit used to measure the voltage between line and neutral of the electric utility.

The method for eliminating the 60Hz component was also straightforward, as a simple high-pass filter was implemented to reduce the magnitude of the undesired 60Hz signal while leaving the voltage distortion with a higher frequency content. The final voltage measurement system is shown in Figure 4-4.

It is important to note that it was necessary to add some preprocessing of the current measurement data due to the fact that the output of the high-pass filter was used for the voltage measurement. This can be illustrated by an example; consider identifying some arbitrary system $U(x; \mu)$ from the parameters $x(t)$ and $y(t)$, as shown in Equation 4.6.

$$x(t)U(x; \mu) = y(t) \qquad (4.3)$$

If there exists some other system $V(x; \gamma)$ which commutes with U, that is to say

$$VU = UV \qquad (4.4)$$

58

then the identification of the system $U(x; \mu)$ is possible with the preprocessed input/output variables $y_p(t) = y(t)V(y; \gamma)$ and $x_p(t) = x(t)V(x; \gamma)$ as long as γ is known.

$$x(t)V(x; \gamma)U(x, \mu) = y(t)V(y; \gamma) \tag{4.5}$$

$$x_p(t)U(x_p; \mu) = y_p(t) \tag{4.6}$$

To relate this example to the experiment under discussion, note that the system to be identified, U, is equivalent to the model of the electric utility, while the parallel of the preprocessing system, V, is the high-pass filter.

This observation implies that it is necessary to filter the current data with a high-pass filter with the same parameters in order to produce voltage and current data which can be used to identify the model of the electric utility. This filtering was done in software with the Matlab routine lsim.

Armed with the data-acquisition procedures described, it is possible to generate the quantities $\hat{v}_s(t)$, $v(t)$, and $i(t)$. As these are the only quantities required to estimate the parameters of the model for the utility (Equation 2.3), it is possible to apply the parameter identification techniques of Chapter 3 to this model. This is presented in the following section.

4.1.2 Results

There were two systems on which the data was cross-validated: a vacuum cleaner and a laser printer. Both of these devices were chosen because of the large currents that they draw at startup.

The first parameter identification method tested was the λ method. Unfortunately, it was found to work extremely poorly for the electric utility. Some of the shortcomings of the λ method were discussed in Chapter 3; the exact reason for failure is uncertain. None of the results obtained by applying this method are therefore presented.

In contrast, the ARMAX method was found to work very well. This can be seen in both of the systems on which the method was cross-validated. The first system presented in this thesis is that of the laser printer. By examining the axes on the plot of the current (Figure 4-5), one might notice that the laser printer draws a fairly significant amount of current on startup. This is due to the heating element in the printer; it periodically needs
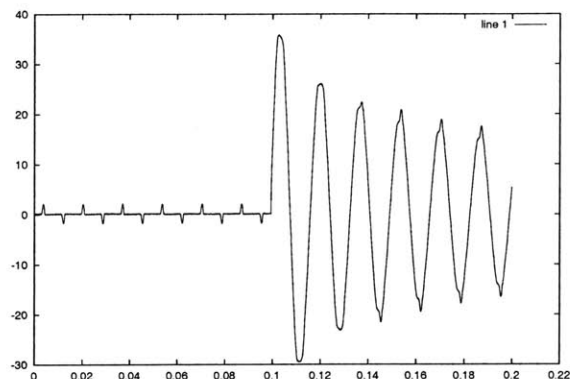
Figure 4-5: Laser printer current transient used to create voltage distortion on the utility. The amplitude is in amps, and the time scale is in seconds.

to heat up the fusing wire which forces the toner to adhere to the paper.

Figure 4-6: Plot of both the measured and the predicted voltage distortion on the electric utility due to a laser printer, as measured directly between line and neutral. The amplitude is measured in volts, while the time scale is measured in seconds.

Figure 4-7: Plot of both the measured and the predicted waveforms representing one cycle of the low-pass filtered $\hat{v}_s(t) - v(t)$ for the laser printer. The axes are labeled similarly.

The two plots in Figures 4-6 and 4-7 illustrate the excellent degree with which the parameters of the model identified by the ARMAX method predicts the voltage distortion due to the large current transient. Figure 4-6 is a plot of the total voltage waveform on the wall, as measured by a high-voltage differential oscilloscope probe; Figure 4-7 is a plot of the predicted and actual voltage that is actually identified. As previously outlined, the high-

pass filtered voltage is collected, and then one distorted voltage cycle $(v_A(t))$ is subtracted from one undistorted cycle $(\hat{v}_s(t))$. The plot of this wavefrom can then be compared to the model output given the current input during the same distorted cycle $(i_A(t))$. It is apparent from comparing these two plots that the discrete-time model is able to predict the voltage waveform to a high degree of accuracy.

The ability of the model to predict the behavior of the vacuum cleaner is equally impressive. The initial current drawn by the motor is close to 100A, and therefore produces a great deal of voltage distortion. The current can be seen in Figure 4-6. The actual and predicted voltage distortion are plotted directly in Figure 4-7.
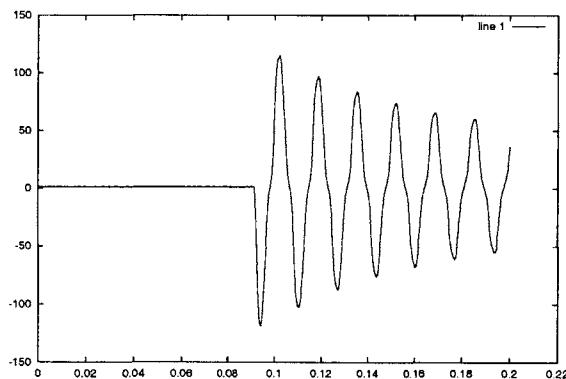
Figure 4-8: Vacuum cleaner current transient used to create voltage distortion on the utility. The amplitude is in amps, and the time scale is in seconds.

The two plots in Figures 4-9 and 4-10 illustrate the same behavior as was described for the laser printer. Note the ability of the model to capture a significant amount of the small-signal voltage distortion (Figure 4-10).

It is clear from these two examples of cross-validation that the ARMAX method worked very well in predicting the voltage distortion introduced by current transients, and that the proposed model of the electric utility accurately describes it.

4.2 The Automobile Chassis

The structure of this section is very similar to that of the electric utility; the test setup used to obtain the characterization data is explained, and the relevant issues that surfaced in the analysis of this data are studied. Lastly, the results of applying the system identification
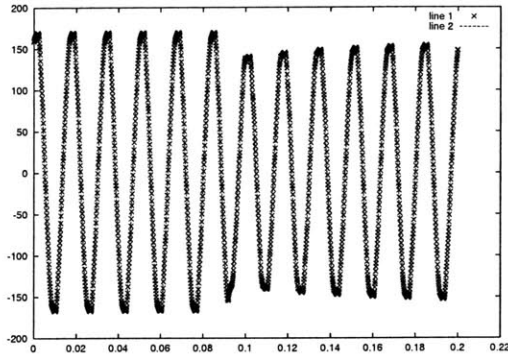
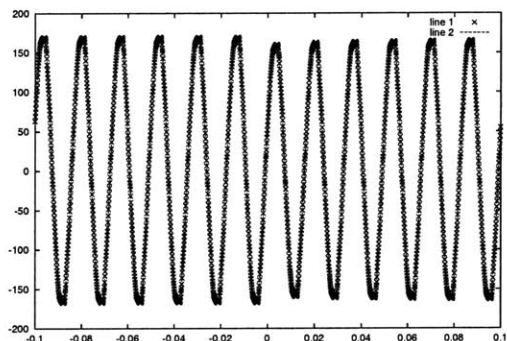Figure 4-9: Plot of both the measured and the predicted voltage distortion on the electric utility due to a vacuum cleaner, as measured directly between line and neutral. The amplitude is measured in volts, while the time scale is measured in seconds.
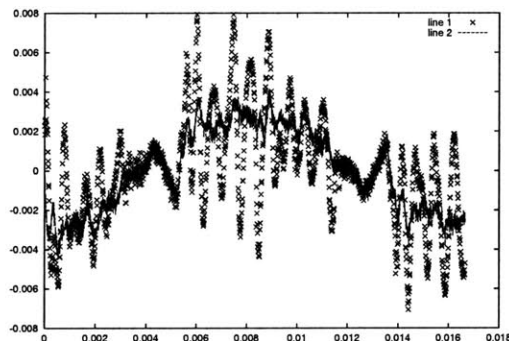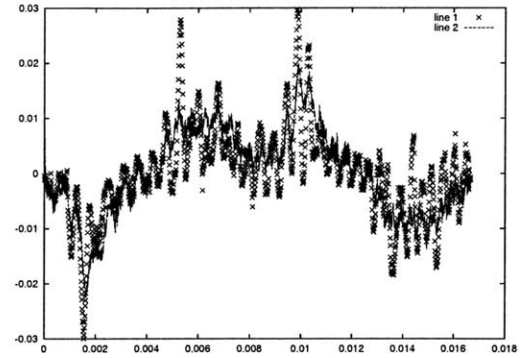

Figure 4-10: Plot of both the measured and the predicted waveforms representing one cycle of the low-pass filtered $\hat{v}_s(t) - v(t)$ for the laser printer. The axes are labeled similarly.

techniques to the model are presented.

4.2.1   Data Collection and Preprocessing

The system for exciting and collecting transients on the automobile chassis was much less complicated than that of the electric utility. In particular, the DC nature of the automobile's electrical system made the process of characterizing the automobile somewhat easier, as the parameters of the model did not have to be fit over a wide range of frequencies. Additionally, many of the difficulties with the electric utility were circumvented by virtue of the fact that the bus voltage in the electrical system is 12V.

In order to measure the effects of voltage distortion on the chassis, it was necessary to inject currents into the car with an amplitude of 15-20A. These currents were injected by a current source similar in design to that which was used on the electric utility. A slightly simplified schematic for this current source is shown in Figure 4-11. This design was chosen because the resistor and capacitor inside the current source would ring with the inductance and resistance of the chassis, thereby manifesting the effects of both elements of the chassis model.

One particular aspect of the component selection for this design deserves mention. Mechanical switches and mosfets in a similar configuration to that which is seen in the schematic
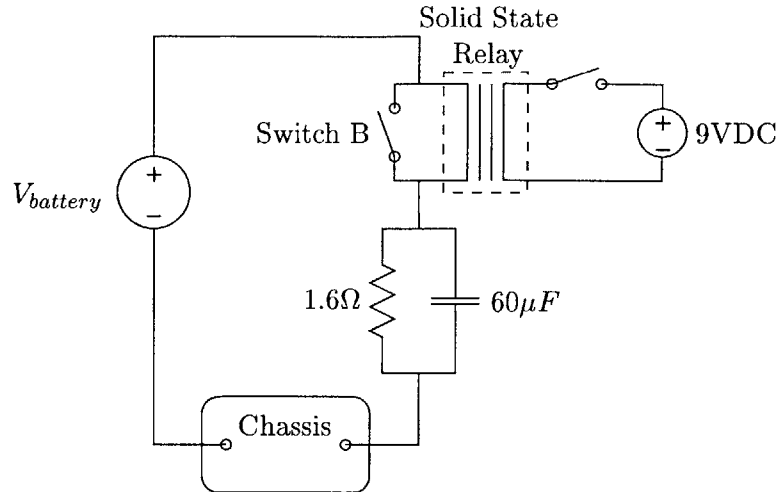
Figure 4-11: Schematic diagram of the test current source used in the experimental setup of the chassis in order to excite current transients.

were initially tested, but these were rejected because of their susceptibility to a phenomenon known as "switch bounce", or the tendency of mechanical switches to repeatedly connect and disconnect ("bounce") for a short period of time after they are closed. This behavior produced extremely noisy and unrepeatable transients. A solid state relay was therefore used because of its immunity to switch bounce; once current starts flowing in the relay, the voltage across the terminals must be set to zero before the relay will turn off. This is accomplished via the commutating switch present in the schematic.

The voltage was then measured between the points on each side of the car (as seen in Figure 2-5). A schematic illustration of this measurement setup is given in Figure 4-12. The current was measured with a Tektronix A6303 current probe and the branch voltages were measured with Tektronix ADA400A differential preamplifiers. One helpful trait of both the current and the voltage measurement devices was the ability to null offsets; as some of the voltage measurements were only a few millivolts, it was important to minimize the offsets introduced by the instruments themselves.

One important property of the chassis was uncovered during the process of recording data. This observation relates to the idea that the test setups during characterization and cross-validation must be similar. In most circumstances, some degree of variation in the system is acceptable between the two processes. As data were acquired for the characterization and cross-validation of the chassis, however, it was discovered that these particular
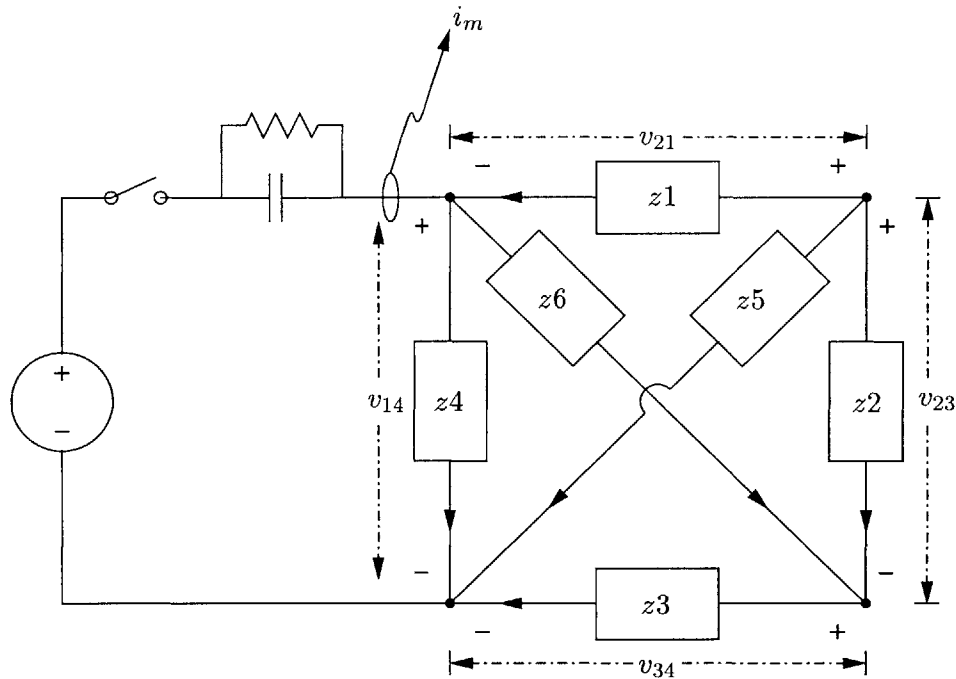
Figure 4-12: An illustration of the experimental setup used to excite transients on the chassis, as well as the voltages and currents measured during the characterization tests.

voltage measurements were extremely sensitive to the magnetic field generated by the steel located in close proximity to the probes. By moving the voltage probes during characterization, or between characterization and cross-validation, the system being modelled effectively changed. This time-varying behavior was not included in the model, thus resulting in models which represented the system very poorly.

Furthermore, the contact resistance of the interface between the probes and the chassis was found to vary widely as the voltage probes were moved. This fact also caused the creation of poor models because the contact resistance was equal to a significant fraction of the chassis resistance.

In order to avoid these pitfalls, a number of steps were taken. The first, and most important, step was to secure and immobilize the voltage probes as far away from the steel as possible, so that the fields would affect them as little as possible (though more than desired) and would not change between experiments. In addition, other ways in which the steel would affect the voltage measurement were avoided through careful cable layout. A diagram of a poor layout of the voltage probes for the differential preamplifier is shown in

Figure 4-13. The magnetic fields due to the presence of the steel in this loop were found to affect the voltage measurement, so care was taken to avoid this layout. Finally, the wires
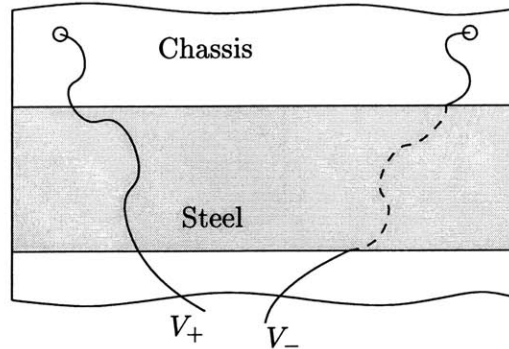
Figure 4-13: Poor voltage probe placement. Notice how the V_+ probe travels over the steel while the V_- probe travels under it, trapping the piece of steel in the loop.

carrying the current from the battery to nodes 1, 2, and 3 were tie-wrapped to the car, so as to prevent the magnetic fields due to the chassis from interfering with the measurement in a variable way.

Very little preprocessing of the data was required for the chassis. Despite the best efforts to the contrary, there were still small DC offsets in some of current and voltage data; these were subtracted off by recording the waveforms at times around the moment the switch was closed. The data were also resampled so that the sampling period was sized appropriately for the process of discrete-time identification, as discussed at the end of §3.2.3.

4.2.2 Results

Upon testing the λ method of system identification, it was found that it did not work very well for the chassis. There are many possible reasons for the failure of the method; one reasonable explanation is that the nonlinear minimization was trying to minimize a residual comprised of only 24 (8 parameters × 3 experiments) different values. Since the method was trying to find the optimal values of twelve different parameters which were nonlinearly related to the 24 parameters obtained via the λ method, it is quite possible that the 24 experimental parameters did not provide enough constraints to successfully find the model parameters. Furthermore, the loss function may have been very poorly formed, with many local minima, so that any expectation of finding a reasonable answer was ill-founded.

Suffice it to say that the λ method did not work well, and that no experimental predictions were obtained with it.

In comparison, the discrete-time identification method worked much better. This can be seen by looking at the following cross-validation plots. This first set of plots was made to demonstrate the ability to which the discrete-time identification method can fit the transient excited by the current source. The current transient which served as the input to the model is given in Figure 4-14, and the predicted and measured voltages are given in Figures 4-15 and 4-16.

Figure 4-14: Current transient injected into node 2 with an excitation from the current source. The time scale is in seconds, and the amplitude is in amps.

These predictions were not performed on the characterization data; rather, they were performed on a separate experiment by using the test current source over the same time scale as the characterization data. The fit of the prediction to the measured data looks remarkably good in the cases of v_{34} and v_{14}, but a comparison of Figure 4-16 to Figure 4-15 might suggest that only some of the voltage waveforms fit well. This is somewhat true, but by noticing that the distortion in Figure 4-15 is between 10mV and 35mV, it is reasonable to expect that simple measurement noise and instrumentation bias is responsible for the degree to which the prediction does not match the measurement. These effects are most likely not as noticeable on v_{34} and v_{14} because the voltage waveforms for prediction are so much larger.

A cross-validation experiment was then carried out with a headlight. The current tran-

66

Figure 4-15: Concatenated plots of v_{21} and v_{23} with an excitation from the current source. The solid line is the actual data, while the dotted line is the prediction. The sampling period is $T = 2\mu s$ and the amplitude is measured in volts.

Figure 4-16: Concatenated plots of v_{34} and v_{14}. The legend is similar.

sient which served as the input to this test is given in Figure 4-17 and the plots of the corresponding voltage distortion are shown in Figures 4-18 and 4-19. It is possible to see that these results are similar; the predictions of v_{34} and v_{14} are very accurate, while the predictions of v_{21} and v_{23} are not quite as accurate. One explanation for the large size of v_{34} and v_{14} to v_{21} and v_{23} is that the measurement of the first two voltages includes the impedance of the bonding strip which ties the chassis to the negative post of the battery, while the second measurement does not. The idea that the bonding strip has a higher impedance than the sheet metal of the automobile chassis is plausible, but this idea has yet to be verified.

The final cross-validation experiment which was performed also used the headlight, but it took place over a longer time scale. Once again, the current transient is shown in Figure 4-20 and the voltage distortion is shown in Figures 4-21 and 4-22. These plots resemble the plots of voltage distortion seen before in their accuracy and behavior, but one point is notable about these plots. The discrete-time identification for the model of the longer time scale had a sampling period of $4\mu s$, but the sampling period for the data in the plots is different - it is $8\mu s$. This fact is somewhat surprising in light of the dependence of the model on the sampling rate of the characterization data, as presented in Figure 3-8. One possible explanation for this phenomenon also exists, however. By realizing that the resistance of

67

the car will dominate as the time scale over which the distortion is examined grows, thus decreasing the dependence of the model on the terms due to inductance, the model will tend to behave more like $v_b[k] = \mathsf{a}_b i_b[k]$. Though this is a plausible argument and is obviously supported by the given data, this fact also has yet to be verified.

Nevertheless, it is clear that the discrete-time identification method is able to capture the parameters of the model well. Moreover, the viability of the proposed model of the automobile chassis has been demonstrated.
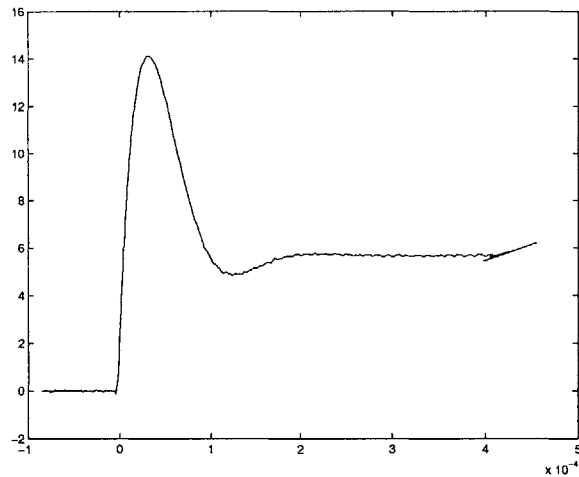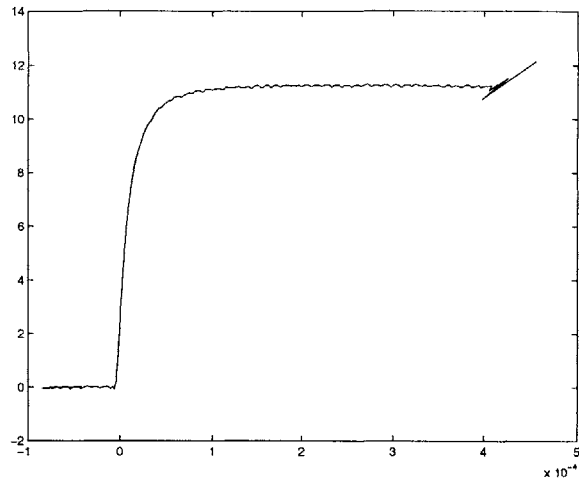
Figure 4-17: Current transient injected into node 2 with an excitation from the headlight. The time scale is in seconds, and the amplitude is in amps.
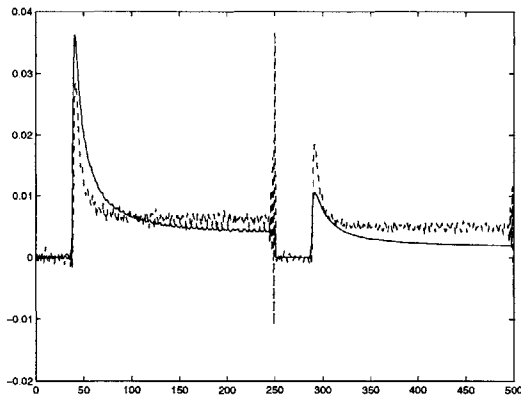
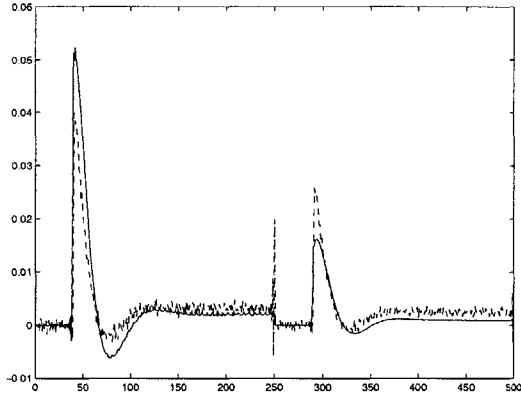

Figure 4-18: Concatenated plots of v_{21} and v_{23} with an excitation from the headlight. The solid line is the actual data, while the dotted line is the prediction. The sampling period is $T = 2\mu s$ and the amplitude is measured in volts.
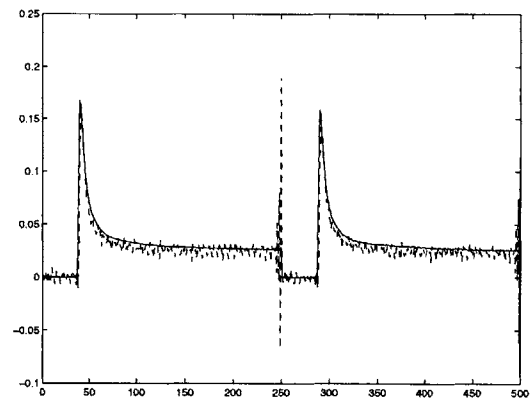
Figure 4-19: Concatenated plots of v_{34} and v_{14}. The legend is similar.

69
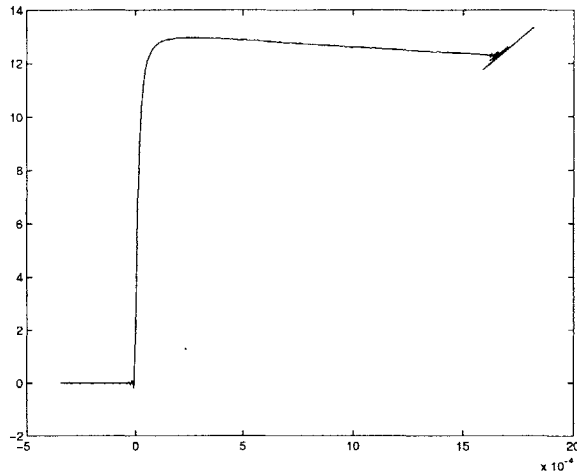
Figure 4-20: Current transient injected into node 2 with an excitation from the headlight over a slightly longer time scale. The time scale is in seconds, and the amplitude is in amps.
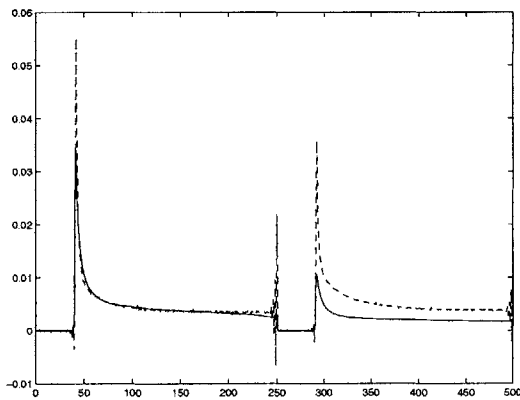
Figure 4-21: Concatenated plots of v_{21} and v_{23} with an excitation from the headlight over a longer timescale. The solid line is the actual data, while the dotted line is the prediction. The sampling period is $T = 8\mu s$ and the amplitude is measured in volts.
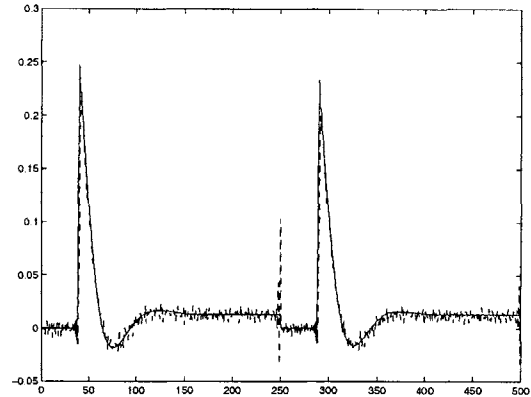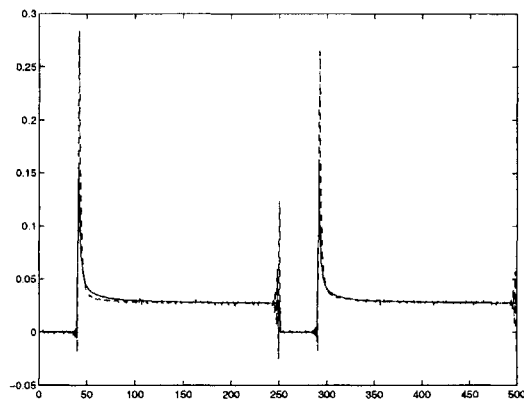

Figure 4-22: Concatenated plots of v_{34} and v_{14}. The legend is similar.

70

Chapter 5

Conclusions

This thesis proposed and verified methods for predicting voltage distortion in two systems in common use today: the electric utility and the automobile. These systems were chosen for analysis because the experimental techniques required to perform the prediction in each system are are somewhat different, as the utility is an AC system and the automobile operates in a DC environment. The possibilities of extending the work done in this thesis to other systems are rich. Furthermore, the nature of predicting voltage distortion as an problem of estimating unknown impedances was discussed.

Physical models were developed for both the electric utility and the automobile chassis. The model for the utility was developed based upon knowledge of the general makeup of the components in a building's electrical system, and this model was further refined with using information acquired from experimental results. A similar model was constructed for the chassis, and this model was also refined by the use of information gathered from experimental data.

A number of different techniques for performing parameter identification were then developed. A continuous-time (λ) method and a discrete-time (ARMAX) method were outlined for use on the electric utility, and the advantages and shortcomings of each method were explored. Similarly, the use of the λ method was proposed for the problem of identifying the parameters of the automobile chassis, and a different discrete-time method of identification was also considered.

Finally, the implementation of the models and parameter identification methods were explored for both systems. It was found that the λ method did not work well, despite its

attractiveness as a continuous-time parameter identification technique. In comparison, the discrete-time identification techniques discussed worked well and suggest further exploration in both systems.

5.1 Further Work

The possibilities are rich for further work in both systems. The method for estimating the impedance of the utility was explored fully at one outlet; further investigation would suggest estimating the impedance at a number of outlets and predicting the voltage distortion at one outlet given a current transient present at another. Furthermore, research should be performed with the goal integrating the estimation work done in this thesis with present research in non-intrusive load monitoring. This would enable the prediction of voltage distortion due to individual load transients at any point in a building through the examination of only the aggregate power flowing into the building.

The possibilities are equally suggestive for further work in predicting voltage distortion on the automobile chassis. A certain amount of work is immediately necessary, for this thesis has only provided a framework for investigation as well as a general proof-of-concept; the refinement of the tools developed is the obvious first step to be undertaken. Another interesting topic might be the investigation of the impedance of a number of cars at various ages; this might result in some interesting findings about the behavior of the automobile electrical system throughout the lifespan of the automobile. Furthermore, the possibility of locating faults and performing diagnostic behavior based upon the voltage transients observed in the automobile has great potential.

Appendix A

Schematics

A.1 The Electric Utility

A.1.1 Current Source
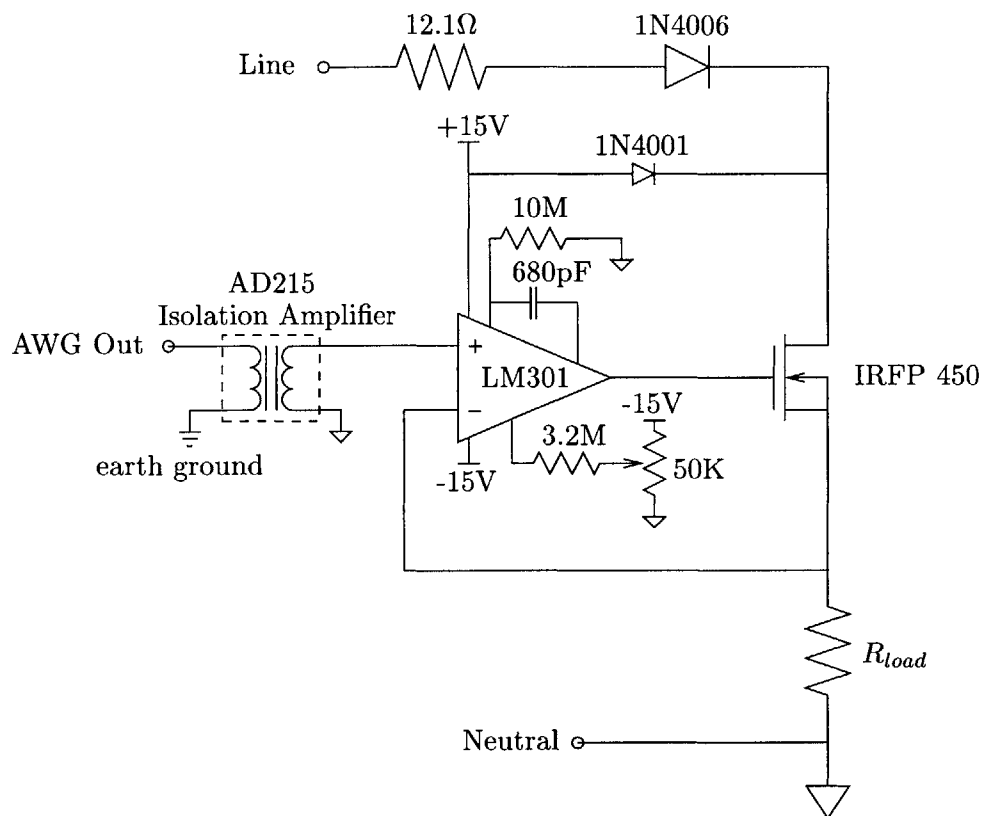
Figure A-1: Current source for the electric utility.

A.1.2 Voltage Measurement Circuit
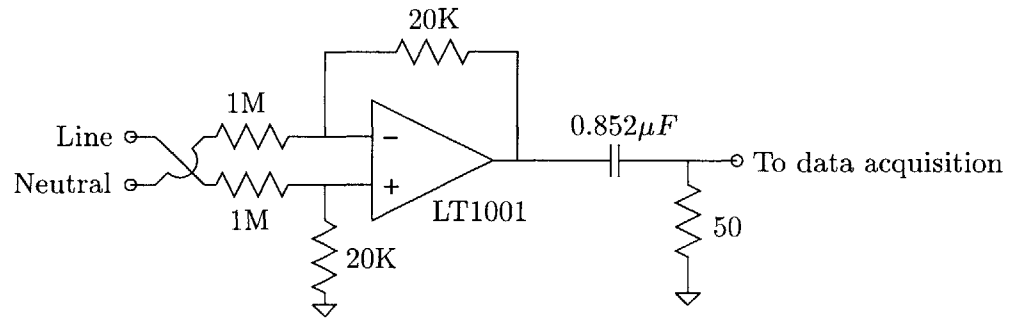
Figure A-2: Voltage measurement circuit for the electric utility.

A.2 The Automobile Chassis

A.2.1 Current Source
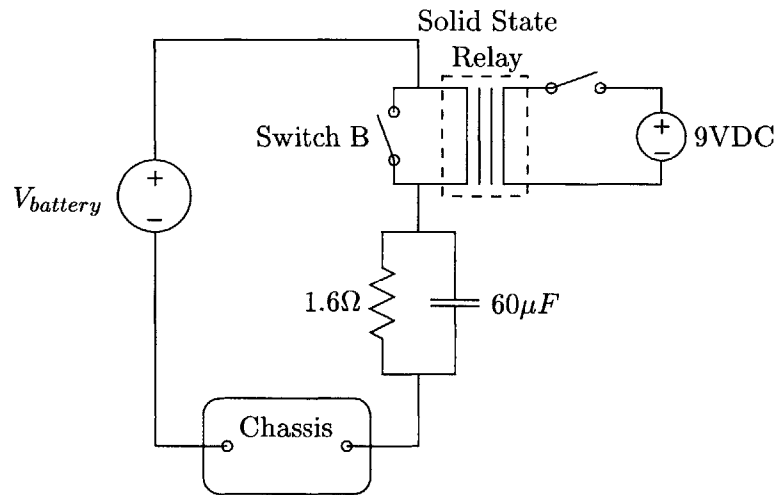
Figure A-3: Characterization current source.

A.2.2 Cross-Validation Source
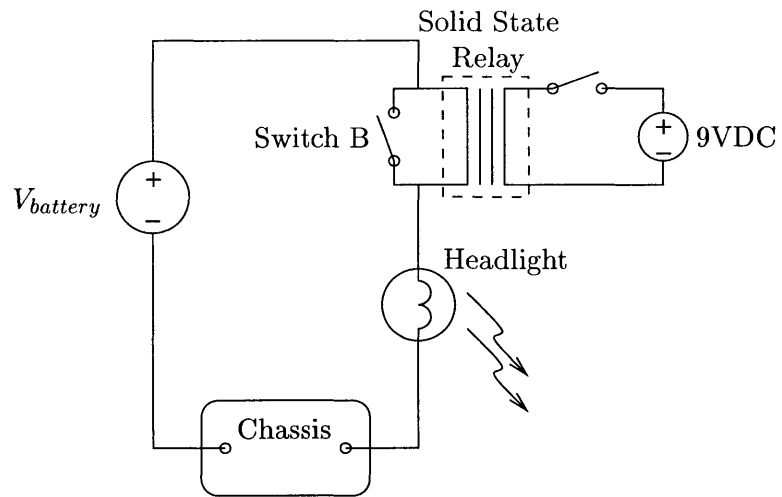
Figure A-4: Characterization current source.

Appendix B

MAPLE Output

This appendix tabulates the set of node equations which describe each experiment. These node equations were written down directly from the schematic diagram given in Figure 2-11. Note that all multiplications as referred to in the results are actually polynomial multiplications; $z5\ z1$ denotes the polynomial multiplication of $(L_5s + R_5)$ and $(L_1s + R_1)$, or $L_1L_5s^2 + (L_1R_5 + L_5R_1)s + R_1R_5$.

Injecting current into node 1; the node equations are:

$$eqn_1 := \frac{v21}{z1} - \frac{v14}{z4} - \frac{v14 - v34}{z6} + it = 0 \tag{B.1}$$

$$eqn_2 := -\frac{v23}{z2} - \frac{v23 + v34}{z5} - \frac{v21}{z1} = 0 \tag{B.2}$$

$$eqn_3 := \frac{v23}{z2} + \frac{v14 - v34}{z6} - \frac{v34}{z3} = 0 \tag{B.3}$$

$$eqn_4 := v14 + v21 - v23 - v34 = 0 \tag{B.4}$$

And the resulting transfer functions are:

$$v_{23} = -it\ \frac{z2\ it\ z4\ (z3\ z1 - z5\ z6)}{\%1} \tag{B.5}$$

77

$$v_{14} = it \, \frac{z4 \, (z3 \, z1 \, z6 + z3 \, z5 \, z1 + z3 \, z2 \, z5 + z5 \, z6 \, z3 + z3 \, z2 \, z1 + z1 \, z6 \, z5 + z5 \, z2 \, z6 + z6 \, z2 \, z1)}{\%1} \tag{B.6}$$

$$v_{34} = it \, \frac{z4 \, it \, z3 \, (z5 \, z1 + z2 \, z5 + z5 \, z6 + z2 \, z1)}{\%1} \tag{B.7}$$

$$v_{21} = -it \, \frac{it \, z4 \, z1 \, (z6 \, z3 + z2 \, z3 + z5 \, z6 + z2 \, z6)}{\%1} \tag{B.8}$$

$$
\begin{aligned}
\%1 \quad = \quad & z3 \, z6 \, z4 + z3 \, z1 \, z6 + z2 \, z3 \, z4 + z1 \, z4 \, z3 + z4 \, z6 \, z5 + z4 \, z2 \, z6 + z3 \, z5 \, z1 \\
= \quad & + z5 \, z6 \, z3 + z3 \, z2 \, z1 + z1 \, z6 \, z5 + z5 \, z2 \, z6 + z6 \, z2 \, z1 + z1 \, z4 \, z5 + z4 \, z2 \, z5 \\
= \quad & + z1 \, z4 \, z2 + z3 \, z2 \, z5
\end{aligned} \tag{B.9}
$$

Injecting a current into node 2; the node equations are:

$$eqn_5 := \frac{v21}{z1} - \frac{v14}{z4} - \frac{v14 - v34}{z6} = 0 \tag{B.10}$$

$$eqn_6 := it - \frac{v23}{z2} - \frac{v23 + v34}{z5} - \frac{v21}{z1} = 0 \tag{B.11}$$

$$eqn_7 := \frac{v23}{z2} + \frac{v14 - v34}{z6} - \frac{v34}{z3} = 0 \tag{B.12}$$

$$eqn_8 := v14 + v21 - v23 - v34 = 0 \tag{B.13}$$

And the resulting transfer functions are:

$$v_{23} = it \, \frac{z2 \, z5 \, (z4 \, z6 + z3 \, z1 + z1 \, z6 + z1 \, z4)}{\%1} \tag{B.14}$$

$$v_{34} = it \, \frac{(z4 \, z2 + z4 \, z6 + z1 \, z4 + z1 \, z6) \, z3 \, z5}{\%1} \tag{B.15}$$

78

$$v_{21} = it \, \frac{z5 \, z1 \, (z2 \, z3 + z2 \, z6 + z4 \, z2 + z6 \, z3)}{\%1} \qquad (B.16)$$

$$v_{14} = it \, \frac{z5 \, z4 \, (z2 \, z3 + z6 \, z3 + z3 \, z1 + z2 \, z6)}{\%1} \qquad (B.17)$$

$$
\begin{aligned}
\%1 \quad = \quad & z3 \, z6 \, z4 + z3 \, z1 \, z6 + z2 \, z3 \, z4 + z1 \, z4 \, z3 + z4 \, z6 \, z5 + z4 \, z2 \, z6 + z3 \, z5 \, z1 \\
= \quad & + z5 \, z6 \, z3 + z3 \, z2 \, z1 + z1 \, z6 \, z5 + z5 \, z2 \, z6 + z6 \, z2 \, z1 + z1 \, z4 \, z5 + z4 \, z2 \, z5 \\
= \quad & + z1 \, z4 \, z2 + z3 \, z2 \, z5 \qquad\qquad (B.18)
\end{aligned}
$$

Finally, injecting a current into node 3, the node equations are:

$$eqn_9 := \frac{v21}{z1} - \frac{v14}{z4} - \frac{v14 - v34}{z6} = 0 \qquad (B.19)$$

$$eqn_{10} := -\frac{v23}{z2} - \frac{v23 + v34}{z5} - \frac{v21}{z1} = 0 \qquad (B.20)$$

$$eqn_{11} := it + \frac{v14 - v34}{z6} - \frac{v34}{z3} + \frac{v23}{z2} = 0 \qquad (B.21)$$

$$eqn_{12} := v14 + v21 - v23 - v34 = 0 \qquad (B.22)$$

And the resulting transfer functions are:

$$v_{23} = -it \, \frac{z3 \, z2 \, it \, (z1 \, z4 + z5 \, z6 + z4 \, z6 + z1 \, z6)}{\%1} \qquad (B.23)$$

$$v_{34} = it \, \frac{(z1 \, z4 \, z5 + z4 \, z2 \, z5 + z1 \, z4 \, z2 + z5 \, z2 \, z6 + z4 \, z6 \, z5 + z4 \, z2 \, z6 + z1 \, z6 \, z5 + z6 \, z2 \, z1) \, z3}{\%1}$$
$$(B.24)$$

$$v_{21} = -it \, \frac{z3 \, z1 \, (z4 \, z2 - z5 \, z6)}{\%1} \qquad (B.25)$$

79

$$v_{14} = it \, \frac{z4 \, z3 \, (z5 \, z1 + z2 \, z5 + z5 \, z6 + z2 \, z1)}{\%1} \qquad \text{(B.26)}$$

$$\begin{aligned}
\%1 \quad &= \quad z3 \, z6 \, z4 + z3 \, z1 \, z6 + z2 \, z3 \, z4 + z1 \, z4 \, z3 + z4 \, z6 \, z5 + z4 \, z2 \, z6 + z3 \, z5 \, z1 \\
&= \quad + z5 \, z6 \, z3 + z3 \, z2 \, z1 + z1 \, z6 \, z5 + z5 \, z2 \, z6 + z6 \, z2 \, z1 + z1 \, z4 \, z5 + z4 \, z2 \, z5 \\
&= \quad + z1 \, z4 \, z2 + z3 \, z2 \, z5 \qquad \text{(B.27)}
\end{aligned}$$

Appendix C

OCTAVE Code

C.1 The λ method example

```
%# dc lambda method

%# pick the initial values of the parameters

R1 = 2.1;
R2 = 2e-2;
L = 12e-6;
C = 10e-6;

%# set up the transfer function for the total impedance

num1 = [R1*C*L (L+R1*R2*C) (R1+R2)];
den1 = [R1*C 1];

%# make the time vector

tt = 0:1:4999;
tt = 1e-7*tt;

%# make the voltage input

vt = [zeros(1, 500) 12*ones(1,4500)];

%# generate the input current

it = lsim(den1, num1, vt, tt);

%# make the transfer function from current to v_out

num2 = [R1*C*L (L+R1*R2*C) R2];
den2 = [R1*C*L (L+R1*R2*C) (R1+R2)];

%# generate v_out
```

```
vi = lsim(num2, den2, vt, tt);

%# add noise to the i_in and v_out, use them as
%# characterization data

itu = it + 0.1*randn(size(vi));
viu = vi + 0.1*randn(size(vi));

%# the lambda method

tau = 5e-5;
lv = lsim(1, [tau 1], viu, tt);
li = lsim(1, [tau 1], itu, tt);

mu = [li lv]  itu;

p = [tau/mu(2) (1-mu(1))/mu(2)];

%# generate the beautiful example plot

plot(tt, itu, tt, lsim(1, p, viu, tt));
```

C.2   The Electric Utility

C.2.1   The λ method

```
% leastsq.m - the script that performs the lambda method estimation

function [final] = leastsq(iin,vin,tin)

tau = 0.002;                         % building parameters for the
lambdanum = [1];                     % least squares fit
lambdaden = [tau 1];
lambda1i = lsim(lambdanum,lambdaden,iin,tin);
lambda2i = lsim(lambdanum,lambdaden,lambda1i,tin);
lambda0i = iin;

lambda1vs = lsim(lambdanum,lambdaden,vin,tin);
lambda2vs = lsim(lambdanum,lambdaden,lambda1vs,tin);

tableau1 = [lambda2i lambda1i lambda0i];    % performing the least squares fit
halfway = tableau1  lambda2vs;

tableau2 = [tau^2 -tau 1;0 tau -2;0 0 1];

final = tableau2  halfway;           % the long sought after answer

residual1 = lambda2vs - tableau1*halfway;
```

```
figure(3);
subplot(211);
plot(residual1);

residual2 = final - tableau2*final;
subplot(212);
plot(residual2);
```

C.2.2 The ARMAX method

```
%
% karakteriz.m - the script which characterizes the electric utility via
% the ARMAX method.
%

% the number of points in a cycle.
N = 12500;

% the scale factor going from the auxiliary current probe to the scope.
% 10mV/div -> 2A/div

scl = 200;

cd dats

R = 50;
C = 0.852e-6;
numfilt = [R*C 0];
denfilt = [R*C 1];

for %k = 1:20

    load -force bart(%k)sv.dat
    load -force bart(%k)i.dat

    va(%k) = interp(bart(%k)sv(:,2), 3);
    ia(%k) = scl*interp(bart(%k)i(:,2), 3);

    t(%k) = bart(%k)i(:, 1);

    t(%k)up = (((1:length(interp(t(%k),3)))*(t(%k)(2)-t(%k)(1))) / 3);
    t(%k)out = t(%k)up(1:N);

    cd ..

    [v(%k)a, ca(%k)] = cyclesub(va(%k),ia(%k),12500);
    [i(%k)f, t(%k)f] = lsim(numfilt,denfilt,c(%k)a,to(%k)ut);

endfor

vf = [v1a' v2a' v3a' v4a' v5a' v6a' v7a' v8a' v9a' v10a' v11a' v12a'
```

```
   v13a' v14a' v15a' v16a' v17a' v18a' v19a' v20a'];

cf = [i1f' i2f' i3f' i4f' i5f' i6f' i7f' i8f' i9f' i10f' i11f' i12f'
 i13f' i14f' i15f' i16f' i17f' i18f' i19f' i20f'];

[nnum, nden] = shazam(vf',cf');

save -ascii karh1.asc nnum nden

%
% shazam.m - the script which performs the ARMAX estimation
%

function [nnum,nden] = shazam(vsigin,csigin)

% Now do that funky state space parameter estimation stuff.

Z = [vsigin csigin];
TH = armax(Z,[2 2 3 0],30);
[nnum,nden] = th2tf(TH);

%
% analyze the data from the laser printer, and produce prediction plots.
%

clear;
hold off;
load -force karh1.asc
plotvar = 1;


% the scale factor for the silly current sensor is sc.

sc = 1000;

cd dats

load laseri.dat
load lasersv.dat
load lasertvd.dat
load lasertvuoff.dat
load lasertvuon.dat

id = sc*laseri(:,2);
svd = lasersv(:,2);
tvdd = lasertvd(:,2);
tvudoff = lasertvuoff(:,2);
tvudon = lasertvuon(:,2);
timed = laseri(:,1);

cd ..

S = 86756;
N = 12500;
sc2 = 120*sqrt(2)/max(tvudon);

idup = interp(id,3);
iup = idup;
```

```
svdup = interp(svd,3);
svup = svdup;

tvddup = interp(tvdd,3);
tvdup = tvddup;

timeup = interp(timed,3);
timep = (1:length(timeup))*((timed(2)-timed(1)) / 3);
timeout = timep(1:N);

iupout = iup(S+1:S+N)-iup(S-4*N+1:S-3*N);
svupout = svup(S+1:S+N)-svup(S-4*N+1:S-3*N);
tvdout = tvdup(S+1:S+N)-tvdup(S-4*N+1:S-3*N);

% make the filter

Rf = 50;
Cf = 0.852e-6;
numf = [Rf*Cf 0];
denf = [Rf*Cf 1];

% plot the unfiltered unsubtracted current

if plotvar == 1
  gset terminal postscript
  gset output "laser_i.ps"
  title('Laser unsubtracted unfiltered current');
  plot(timep,iup);
else
  figure(1)
  title('Laser unsubtracted unfiltered current');
  plot(timep,iup);
end

% plot the unfiltered subtracted current

if plotvar == 1
  gset terminal postscript
  gset output "laser_is.ps"
  title('Laser subtracted unfiltered current');
  plot(timeout,iupout);
else
  figure(2)
  title('Laser subtracted unfiltered current');
  plot(timeout,iupout);
end

% plot the filtered subtracted current

[iupfilt,x] = lsim(numf,denf,iupout,timeout);

if plotvar == 1
  gset terminal postscript
  gset output "laser_isf.ps"
  title('Laser filtered subtracted current');
  plot(timeout,iupfilt);
else
  figure(3)
  title('Laser filtered subtracted current');
```

85

```
    plot(timeout,iupfilt);
end

% plot the unfiltered unsubtracted total voltage

if plotvar == 1
  gset terminal postscript
  gset output "laser_tv.ps"
  title('Laser unfiltered unsubtracted total voltage');
  plot(timep,sc2*tvdup);
else
  figure(4)
  title('Laser unfiltered unsubtracted total voltage');
  plot(timep,sc2*tvdup);
end

% plot the filtered unsubtracted total voltage

%[tvdfilt,x] = lsim(numf,denf,tvdup,timep);

%if plotvar == 1
%   gset terminal postscript
%   gset output "laser_tvf.ps"
%   title('Laser filtered unsubtracted total voltage');
%   plot(timep,tvdfilt);
%else
%   figure(5)
%   title('Laser filtered unsubtracted total voltage');
%   plot(timep,tvdfilt);
%end

% plot the experimentally filtered subtracted voltage

if plotvar == 1
  gset terminal postscript
  gset output "laser_svf.ps"
  title('Laser experimentally filtered subtracted voltage');
  plot(timeout,svupout);
else
  figure(6)
  title('Laser experimentally filtered subtracted voltage');
  plot(timeout,svupout);
end

s_estimate = dlsim(nnum,nden,iupfilt);

if plotvar == 1
  gset terminal postscript
  gset output "laser_svpred.ps"
  title('Laser predicted/real voltage distortion');
  plot(timeout,svupout,timeout,s_estimate);
else
  figure(7)
  title('Laser predicted/real voltage distortion');
  plot(timeout,svupout,timeout,s_estimate);
end

% now try to predict the total voltage distortion.
```

```
t_estimate = dlsim(nnum,nden,id);
tvpred = tvudon+t_estimate;

if plotvar == 1
  gset terminal postscript
  gset output "laser_tvpred.ps"
  title('Laser real/predicted total voltage distortion')
  plot(timed,sc2*tvdd,timed,sc2*tvpred);
else
  figure(1)
  title('Laser real/predicted total voltage distortion')
  plot(timed,sc2*tvdd,timed,sc2*tvpred);
end

%
% analyze the data from the vacuum, and produce prediction plots.
%

clear;
hold off;
load -force karh1.asc
plotvar = 1;

% the scale factor for the silly current sensor is sc.

sc = 5000;

cd dats

load vaci.dat
load vacsv.dat
load vactvd.dat
load vactvu.dat

id = sc*vaci(:,2);
svd = vacsv(:,2);
tvdd = vactvd(:,2);
tvud = vactvu(:,2);
timed = vaci(:,1);

cd ..

S = 85945;
N = 12500;
sc2 = 120*sqrt(2)/max(tvud);

idup = interp(id,3);
iup = idup;

svdup = interp(svd,3);
svup = svdup;

tvddup = interp(tvdd,3);
tvdup = tvddup;

timeup = interp(timed,3);
timep = (1:length(timeup))*((timed(2)-timed(1)) / 3);
timeout = timep(1:N);
```

```
iupout = iup(S+1:S+N)-iup(S-4*N+1:S-3*N);
svupout = svup(S+1:S+N)-svup(S-4*N+1:S-3*N);
tvdout = tvdup(S+1:S+N)-tvdup(S-4*N+1:S-3*N);

% make the filter

Rf = 50;
Cf = 0.852e-6;
numf = [Rf*Cf 0];
denf = [Rf*Cf 1];

% plot the unfiltered unsubtracted current

if plotvar == 1
  gset terminal postscript
  gset output "vac_i.ps"
  title('Vacuum unsubtracted unfiltered current');
  plot(timep,iup);
else
  figure(1)
  title('Vacuum unsubtracted unfiltered current');
  plot(timep,iup);
end

% plot the unfiltered subtracted current

if plotvar == 1
  gset terminal postscript
  gset output "vac_is.ps"
  title('Vacuum subtracted unfiltered current');
  plot(timeout,iupout);
else
  figure(2)
  title('Vacuum subtracted unfiltered current');
  plot(timeout,iupout);
end

% plot the filtered subtracted current

[iupfilt,x] = lsim(numf,denf,iupout,timeout);

if plotvar == 1
  gset terminal postscript
  gset output "vac_isf.ps"
  title('Vacuum filtered subtracted current');
  plot(timeout,iupfilt);
else
  figure(3)
  title('Vacuum filtered subtracted current');
  plot(timeout,iupfilt);
end

% plot the unfiltered unsubtracted total voltage

if plotvar == 1
  gset terminal postscript
  gset output "vac_tv.ps"
  title('Vacuum unfiltered unsubtracted total voltage');
  plot(timep,sc2*tvdup);
```

88

```
else
  figure(4)
  title('Vacuum unfiltered unsubtracted total voltage');
  plot(timep,sc2*tvdup);
end

% plot the filtered unsubtracted total voltage

%[tvdfilt,x] = lsim(numf,denf,tvdup,timep);

%if plotvar == 1
%  gset terminal postscript
%  gset output "vac_tvf.ps"
%  title('Vacuum filtered unsubtracted total voltage');
%  plot(timep,tvdfilt);
%else
%  figure(5)
%  title('Vacuum filtered unsubtracted total voltage');
%  plot(timep,tvdfilt);
%end

% plot the experimentally filtered subtracted voltage

if plotvar == 1
  gset terminal postscript
  gset output "vac_svf.ps"
  title('Vacuum experimentally filtered subtracted voltage');
  plot(timeout,svupout);
else
  figure(6)
  title('Vacuum experimentally filtered subtracted voltage');
  plot(timeout,svupout);
end

s_estimate = dlsim(nnum,nden,iupfilt);

if plotvar == 1
  gset terminal postscript
  gset output "vac_svpred.ps"
  title('Vacuum predicted/real voltage distortion');
  plot(timeout,svupout,timeout,s_estimate);
else
  figure(7)
  title('Vacuum predicted/real voltage distortion');
  plot(timeout,svupout,timeout,s_estimate);
end

% now try to predict the total voltage distortion.

t_estimate = dlsim(nnum,nden,idup);
tvpred = interp(tvud,3)+t_estimate;

if plotvar == 1
  gset terminal postscript
  gset output "vac_tvpred.ps"
  title('Vacuum real/predicted total voltage distortion')
  plot(timep,sc2*tvdup,timep,sc2*tvpred);
else
  figure(8)
```

89

```
  title('Vacuum real/predicted total voltage distortion')
  plot(timep,sc2*tvdup,timep,sc2*tvpred);
end
```

C.3   The Automobile Chassis

C.3.1   The λ method

```
%#
%# 6 branch estimation via the lambda method
%#

clear

%# load data

dataload

%# define functions

function out = tconv(x1, x2, x3)
  out = conv(x1, conv(x2, x3));
endfunction

function out = fconv(x1, x2, x3, x4)
  out = conv(x1, conv(x2, conv(x3, x4)));
endfunction

function out = lambdae(data, time, tau)

  num = 1; den = [tau 1];

  [ld, garbage] = lsim(num, den, data, time);
  [lld, garbage] = lsim(num, den, ld, time);
  [llld, garbage] = lsim(num, den, lld, time);
  [lllld, garbage] = lsim(num, den, llld, time);

  out = [lllld llld lld ld data];

endfunction

%# lossfn1 for polynomial f(s) of the form
%#
%# f(s) = s^4 + mu1*s^3 + ... + mu4
%#        ------------------------
%#             mu5*s^3 + ... + mu8
```

```
function out = lossfn1(mu, nv, dv, tau)

  out = [( (4 - mu(4)) / tau ) - nv(2)/nv(1);
  ( (6 - mu(3) - 3*mu(4)) / tau^2 ) - nv(3)/nv(1);
  ( (4 - mu(2) - 2*mu(3) - 3*mu(4)) / tau^3 ) - nv(4)/nv(1);
  ( (1 - mu(1) - mu(2) - mu(3) - mu(4)) / tau^4 ) - nv(5)/nv(1);
  ( mu(8) / tau ) - dv(1)/nv(1);
  ( (mu(7) + 3*mu(8)) / tau^2 ) - dv(2)/nv(1);
  ( (mu(6) + 2*mu(7) + 3*mu(8)) / tau^3 ) - dv(3)/nv(1);
  ( (mu(5) + mu(6) + mu(7) + mu(8)) / tau^4 ) - dv(4)/nv(1)];

endfunction


function out = lossfn1a(mu, tau)

  out = [( (4 - mu(4)) / tau );
  ( (6 - mu(3) - 3*mu(4)) / tau^2 );
  ( (4 - mu(2) - 2*mu(3) - 3*mu(4)) / tau^3 );
  ( (1 - mu(1) - mu(2) - mu(3) - mu(4)) / tau^4 );
  ( mu(8) / tau );
  ( (mu(7) + 3*mu(8)) / tau^2 );
  ( (mu(6) + 2*mu(7) + 3*mu(8)) / tau^3 );
  ( (mu(5) + mu(6) + mu(7) + mu(8)) / tau^4 )];

endfunction



%# lossfn2 for polynomial f(s) of the form
%#
%# f(s) = mu1*s^3 + ... + mu4
%#        -------------------
%#           s^3 + ... + mu7

function out = lossfn2(mu, nv, dv, tau)

  out = [ mu(4) - nv(1)/dv(1);
  (mu(3) + 3*mu(4))/tau - nv(2)/dv(1);
  (mu(2) + 2*mu(3) + 3*mu(4))/tau^2 - nv(3)/dv(1);
  (mu(1) + mu(2) + mu(3) + mu(4))/tau^3 - nv(4)/dv(1);
  (3 - mu(7))/tau - dv(2)/dv(1);
  (6 - 2*mu(7) - mu(6))/tau^2 - dv(3)/dv(1);
  (4 - mu(7) - mu(6) - mu(5))/tau^3 - dv(4)/dv(1)];

endfunction

function out = lossfn2a(mu, tau)

  out = [ mu(4);
  (mu(3) + 3*mu(4))/tau;
  (mu(2) + 2*mu(3) + 3*mu(4))/tau^2;
  (mu(1) + mu(2) + mu(3) + mu(4))/tau^3;
  (3 - mu(7))/tau;
  (6 - 2*mu(7) - mu(6))/tau^2;
  (4 - mu(7) - mu(6) - mu(5))/tau^3];

endfunction

function mu = lambdaize(it, vt, tt, tau);
```

```
    num = 1; den = [tau 1];

    [lv, garbage] = lsim(num, den, vt, tt);
    [li, garbage] = lsim(num, den, it, tt);

    mup = [li lv]  it;

    mu = [tau/mup(2) (1-mup(1))/mup(2)];

endfunction


%# DC METHOD : RESISTANCE

%# experiment 1

function out = getrsfrom1(x, i1, tv)

    v341 = tv(:,1); v231 = tv(:,2);
    v121 = tv(:,3); v141 = tv(:,4);

    r1 = x(1); r2 = x(2);
    r3 = x(3); r4 = x(4);
    r5 = x(5); r6 = x(6);

    range = 4001:5000;
    v34 = v341(range);
    v23 = v231(range);
    v12 = v121(range);
    v14 = v141(range);
    i1a = i1(range);

    n34 = -(r5*r2*r3 + r5*r1*r3 + r2*r1*r3 + r6*r3*r5 - r5*r2*r6)*r4;
    d1 = (-r3*r4*r6 + r4*r2*r6 - r3*r1*r6 + r1*r6*r2 - r4*r2*r3 - r3*r1*r4 + r1*r4*r2 - r5*r2*r3 - r5*r1*r3 -
    v34i1 = n34/d1;

    n23 = r1*r4*r3*r2;
    v23i1 = n23/d1;

    n14 = r4*(-r3*r1*r6 + r1*r6*r2 - r5*r2*r3 - r5*r1*r3 - r2*r1*r3 - r6*r3*r5 + r5*r2*r6);
    v14i1 = n14/d1;

    n12 = r4*r1*(-r6*r3+r2*r6-r2*r3);
    v12i1 = n12/d1;

    out = [v34 - v34i1*i1a;
   v23 - v23i1*i1a;
   v14 - v14i1*i1a;
   v12 - v12i1*i1a];

endfunction

%# experiment 2

function out = getrsfrom2(x, i2, tv)

    v342 = tv(:,1); v232 = tv(:,2);
    v212 = tv(:,3); v142 = tv(:,4);
```

```
r1 = x(1); r2 = x(2);
r3 = x(3); r4 = x(4);
r5 = x(5); r6 = x(6);

range = 4001:5000;
v34 = v342(range);
v23 = v232(range);
v21 = v212(range);
v14 = v142(range);
i2a = i2(range);

n23 = r2*r5*(r4*r6 + r3*r1 + r1*r6 + r1*r4);
d2 = (r3*r4*r6 + r3*r1*r6 + r3*r1*r4 + r2*r1*r3 + r5*r1*r3 + r4*r2*r3 + r4*r5*r6 + r4*r2*r6 + r5*r2*r3 + r
v23i2 = n23/d2;

n34 = (r4*r2 + r4*r6 + r1*r4 + r1*r6)*r3*r5;
v34i2 = n34/d2;

n14 = r5*r4*(r2*r3 + r6*r3 + r3*r1 + r2*r6);
v14i2 = n14/d2;

n21 = r5*r1*(r2*r3 + r2*r6 + r4*r2 + r6*r3);
v21i2 = n21/d2;

out = [v23 - v23i2*i2a;
v34 - v34i2*i2a;
v14 - v14i2*i2a;
v21 - v21i2*i2a];

endfunction

%# experiment 3

function out = getrsfrom3(x, i3, tv)

v343 = tv(:,1); v323 = tv(:,2);
v213 = tv(:,3); v143 = tv(:,4);

r1 = x(1); r2 = x(2);
r3 = x(3); r4 = x(4);
r5 = x(5); r6 = x(6);

range = 4001:5000;
v34 = v343(range);
v32 = v323(range);
v21 = v213(range);
v14 = v143(range);
i3a = i3(range);

n32 = r3*r2*(r4*r6 + r5*r6 + r1*r6 + r1*r4);
d3 = (r3*r4*r6 + r3*r1*r6 + r3*r1*r4 + r2*r1*r3 + r5*r1*r3 + r4*r2*r3 + r4*r5*r6 + r4*r2*r6 + r5*r2*r3 + r
v32i3 = n32/d3;

n34 = (r1*r4*r2 + r4*r2*r5 + r1*r4*r5 + r4*r2*r6 + r1*r5*r6 + r4*r5*r6 + r5*r2*r6 +r1*r6*r2)*r3;
v34i3 = n34/d3;

n14 = r3*r4*(r2*r1 + r1*r5 + r2*r5 + r5*r6);
v14i3 = n14/d3;
```

93

```
  n21 = r3*r1*(r5*r6 - r4*r2);
  v21i3 = n21/d3;

  out = [v32 - v32i3*i3a;
 v34 - v34i3*i3a;
 v14 - v14i3*i3a;
 v21 - v21i3*i3a];

endfunction

function out = getrs(z, tv, ti)

  tv1 = tv(:,1:4);
  tv2 = tv(:,5:8);
  tv3 = tv(:,9:12);

  i1 = ti(:,1);
  i2 = ti(:,2);
  i3 = ti(:,3);

  x = 1e-3*z;

  out = [getrsfrom1(x, i1, tv1);
 getrsfrom2(x, i2, tv2);
 getrsfrom3(x, i3, tv3)];

endfunction

tv1 = [v341 v231 v121 v141];
tv2 = [v342 v232 v212 v142];
tv3 = [v343 v323 v213 v143];

tv = [tv1 tv2 tv3];
ti = [i1 i2 i3];

gaussnewton_options("epsfcn", 1e-4);
gaussnewton_options("ftol", 1e-4);
[rs, fvec, info, nfev] = lmrecipes('getrs', ones(6,1), tv, ti);

rs = 1e-3*rs
save -ascii rp rs


%# LAMBDA METHOD : INDUCTANCE

%# VOLTAGE -> CURRENT

%# experiment 1

tau = 5e-6;

li1 = lambdae(i1, t1, tau);
lv341 = lambdae(v341, t1, tau);
lv231 = lambdae(v231, t1, tau);
lv121 = lambdae(v121, t1, tau);
lv141 = lambdae(v141, t1, tau);

A341 = [li1(:,1:4) lv341(:,1:4)];
b = li1(:,5);
```

```
mu341 = A341  b;

A231 = [1i1(:,1:4) 1v231(:,1:4)];
mu231 = A231  b;

A121 = [1i1(:,1:4) 1v121(:,1:4)];
mu121 = A121  b;

A141 = [1i1(:,1:4) 1v141(:,1:4)];
mu141 = A141  b;

function out = getlsfrom1b(x, rs, mus, tau)

   mu341 = mus(:,1);   mu231 = mus(:,2);
   mu121 = mus(:,3);   mu141 = mus(:,4);

   11 = x(1); 12 = x(2);
   13 = x(3); 14 = x(4);
   15 = x(5); 16 = x(6);

   r1 = rs(1); r2 = rs(2);
   r3 = rs(3); r4 = rs(4);
   r5 = rs(5); r6 = rs(6);

   z1 = [11 r1]; z2 = [12 r2];
   z3 = [13 r3]; z4 = [14 r4];
   z5 = [15 r5]; z6 = [16 r6];

   n34 = -conv(z4, (tconv(z5, z2, z3) + tconv(z5, z1, z3) + tconv(z2, z1, z3) + tconv(z6, z3, z5) - tconv(z5,

   d1 = (-tconv(z3, z4, z6) + tconv(z4, z2, z6) - tconv(z3, z1, z6) + tconv(z1, z6, z2) - tconv(z4, z2, z3) -

   n23 = fconv(z1, z2, z3, z4);

   n14 = conv(z4, (-tconv(z3, z1, z6) + tconv(z1, z6, z2) - tconv(z5, z2, z3) - tconv(z5, z1, z3) - tconv(z2,

   n12 = tconv(z4, z1, (-conv(z6, z3) + conv(z2, z6) - conv(z2, z3)));

   out = [lossfn1(mu341, n34, d1, tau);
 lossfn1(mu121, n12, d1, tau);
%# lossfn1(mu231, n23, d1, tau);
 lossfn1(mu141, n14, d1, tau)];

endfunction

%# experiment 2

1i2 = lambdae(i2, t2, tau);
1v342 = lambdae(v342, t2, tau);
1v232 = lambdae(v232, t2, tau);
1v212 = lambdae(v212, t2, tau);
1v142 = lambdae(v142, t2, tau);

A342 = [1i2(:,1:4) 1v342(:,1:4)];
b = 1i2(:,5);
mu342 = A342  b;

A232 = [1i2(:,1:4) 1v232(:,1:4)];
mu232 = A232  b;
```

```
A212 = [li2(:,1:4) lv212(:,1:4)];
mu212 = A212 b;

A142 = [li2(:,1:4) lv142(:,1:4)];
mu142 = A142 b;



function out = getlsfrom2b(x, rs, mus, tau)

  mu342 = mus(:,1);   mu232 = mus(:,2);
  mu212 = mus(:,3);   mu142 = mus(:,4);

  l1 = x(1); l2 = x(2);
  l3 = x(3); l4 = x(4);
  l5 = x(5); l6 = x(6);

  r1 = rs(1); r2 = rs(2);
  r3 = rs(3); r4 = rs(4);
  r5 = rs(5); r6 = rs(6);

  z1 = [l1 r1]; z2 = [l2 r2];
  z3 = [l3 r3]; z4 = [l4 r4];
  z5 = [l5 r5]; z6 = [l6 r6];

  n23 = tconv(z2, z5, (conv(z4, z6) + conv(z3, z1) + conv(z1, z6) + conv(z1, z4) ) );

  d2 = tconv(z3, z4, z6) + tconv(z1, z3, z6) + tconv(z1, z3, z4) + tconv(z1, z2, z3) + tconv(z5, z1, z3) +

  n34 = tconv(z3, z5, (conv(z4, z2) + conv(z4, z6) + conv(z1, z4) + conv(z1, z6) ) );

  n14 = tconv(z4, z5, (conv(z2, z3) + conv(z3, z6) + conv(z1, z3) + conv(z2, z6) ) );

  n21 = tconv(z1, z5, (conv(z2, z3) + conv(z2, z6) + conv(z2, z4) + conv(z3, z6) ) );

  out = [lossfn1(mu342, n34, d2, tau);
 lossfn1(mu142, n14, d2, tau);
 lossfn1(mu232, n23, d2, tau);
 lossfn1(mu212, n21, d2, tau)];

endfunction

%# experiment 3

li3 = lambdae(i3, t3, tau);
lv343 = lambdae(v343, t3, tau);
lv323 = lambdae(v323, t3, tau);
lv213 = lambdae(v213, t3, tau);
lv143 = lambdae(v143, t3, tau);

A343 = [li3(:,1:4) lv343(:,1:4)];
b = li3(:,5);
mu343 = A343 b;

A323 = [li3(:,1:4) lv323(:,1:4)];
mu323 = A323 b;

A213 = [li3(:,1:4) lv213(:,1:4)];
mu213 = A213 b;
```

96

```
A143 = [li3(:,1:4) lv143(:,1:4)];
mu143 = A143 \ b;

function out = getlsfrom3b(x, rs, mus, tau)

  mu343 = mus(:,1);  mu323 = mus(:,2);
  mu213 = mus(:,3);  mu143 = mus(:,4);

  l1 = x(1); l2 = x(2);
  l3 = x(3); l4 = x(4);
  l5 = x(5); l6 = x(6);

  r1 = rs(1); r2 = rs(2);
  r3 = rs(3); r4 = rs(4);
  r5 = rs(5); r6 = rs(6);

  z1 = [l1 r1]; z2 = [l2 r2];
  z3 = [l3 r3]; z4 = [l4 r4];
  z5 = [l5 r5]; z6 = [l6 r6];

  n32 = tconv(z3, z2, (conv(z4, z6) + conv(z5, z6) + conv(z1, z6) + conv(z1, z4) ) );

  d3 = tconv(z3, z4, z6) + tconv(z3, z1, z6) + tconv(z3, z1, z4) + tconv(z2, z1, z3) + tconv(z5, z1, z3) + t

  n34 = conv(z3, ( tconv(z1, z4, z2) + tconv(z4, z2, z5) + tconv(z1, z4, z5) + tconv(z4, z2, z6) + tconv(z1,

  n14 = tconv(z3, z4, (conv(z2, z1) + conv(z1, z5) + conv(z2, z5) + conv(z5, z6) ) );

  n21 = tconv(z3, z1, (conv(z5, z6) - conv(z4, z2) ) );

  out = [lossfn1(mu323, n32, d3, tau);
lossfn1(mu143, n14, d3, tau);
lossfn1(mu343, n34, d3, tau);
lossfn1(mu213, n21, d3, tau)];

endfunction

function out = getlsb(z, rs, mus, tau)

  mu1 = mus(:,1:4);
  mu2 = mus(:,5:8);
  mu3 = mus(:,9:12);

  x = 1e-6*z;

  out = [getlsfrom1b(x, rs, mu1, tau);
getlsfrom2b(x, rs, mu2, tau);
getlsfrom3b(x, rs, mu3, tau)];

endfunction

mu1 = [mu341 mu231 mu121 mu141];
mu2 = [mu342 mu232 mu212 mu142];
mu3 = [mu343 mu323 mu213 mu143];
mus = [mu1 mu2 mu3];

gaussnewton_options("epsfcn", 1e-4);
gaussnewton_options("ftol", 1e-4);
```

```
[lp4, fvec, info, nfev] = lmrecipes('getlsb', ones(6,1), rs, mus, tau);

lp4 = 1e-6*lp4;
save -ascii 6bp4 lp4 rs


%# LAMBDA METHOD : RESISTANCE AND INDUCTANCE
%# VOLTAGE -> CURRENT

%# experiment 1

tau1 = 5e-6;

smu341 = lambdaize(i1, v341, t1, tau1);
smu121 = lambdaize(i1, v121, t1, tau1);
smu141 = lambdaize(i1, v141, t1, tau1);

plot(t1, i1, t1, lsim(1, smu341, v341, t1))
plot(t1, i1, t1, lsim(1, smu141, v141, t1))
plot(t1, i1, t1, lsim(1, smu121, v121, t1))

plot(ct1, ci1, ct1, lsim(1, smu341, cv341, ct1))
plot(ct1, ci1, ct1, lsim(1, smu141, cv141, ct1))
plot(ct1, ci1, ct1, lsim(1, smu121, cv121, ct1))

%# experiment 2

tau2 = 5e-6;

smu142 = lambdaize(i2, v142, t2, tau2);
smu212 = lambdaize(i2, v212, t2, tau2);
smu232 = lambdaize(i2, v232, t2, tau2);
smu342 = lambdaize(i2, v342, t2, tau2);
smua = lambdaize(i2, v142+v212, t2, tau2);
smub = lambdaize(i2, v232+v342, t2, tau2);

plot(t2, i2, t2, lsim(1, smu142, v142, t2))
plot(t2, i2, t2, lsim(1, smu212, v212, t2))
plot(t2, i2, t2, lsim(1, smu232, v232, t2))
plot(t2, i2, t2, lsim(1, smu342, v342, t2))
plot(t2, i2, t2, lsim(1, smua, v142+v212, t2))
plot(t2, i2, t2, lsim(1, smub, v232+v342, t2))

plot(ct2, ci2, ct2, lsim(1, smu142, cv142, ct2))
plot(ct2, ci2, ct2, lsim(1, smu212, cv212, ct2))
plot(ct2, ci2, ct2, lsim(1, smu232, cv232, ct2))
plot(ct2, ci2, ct2, lsim(1, smu342, cv342, ct2))

%# experiment 3

tau3 = 5e-6;

smu143 = lambdaize(i3, v143, t3, tau3);
smu213 = lambdaize(i3, v213, t3, tau3);
smu323 = lambdaize(i3, v323, t3, tau3);
smu343 = lambdaize(i3, v343, t3, tau3);

plot(t3, i3, t3, lsim(1, smu143, v143, t3));
plot(t3, i3, t3, lsim(1, smu143, v143, t3));
```

```
plot(t3, i3, t3, lsim(1, smu143, v143, t3));
plot(t3, i3, t3, lsim(1, smu143, v143, t3));

plot(ct3, ci3, ct3, lsim(1, smu143, cv143, ct3));
plot(ct3, ci3, ct3, lsim(1, smu143, cv143, ct3));
plot(ct3, ci3, ct3, lsim(1, smu143, cv143, ct3));
plot(ct3, ci3, ct3, lsim(1, smu143, cv143, ct3));


%# INTERMEDIATE VERIFICATION : LAMBDA
%# VOLTAGE -> CURRENT

%# experiment 1

tau1 = 5e-6;

li1 = lambdae(i1, t1, tau1);
lv341 = lambdae(v341, t1, tau1);
lv231 = lambdae(v231, t1, tau1);
lv121 = lambdae(v121, t1, tau1);
lv141 = lambdae(v141, t1, tau1);

A341 = [li1(:,1:4) lv341(:,1:4)];
b = li1(:,5);
mu341 = A341  b;

A231 = [li1(:,1:4) lv231(:,1:4)];
mu231 = A231  b;

A121 = [li1(:,1:4) lv121(:,1:4)];
mu121 = A121  b;

A141 = [li1(:,1:4) lv141(:,1:4)];
mu141 = A141  b;

cli1 = lambdae(ci1, ct1, tau1);
clv341 = lambdae(cv341, ct1, tau1);
clv231 = lambdae(cv231, ct1, tau1);
clv121 = lambdae(cv121, ct1, tau1);
clv141 = lambdae(cv141, ct1, tau1);

cA341 = [cli1(:,1:4) clv341(:,1:4)];
cA231 = [cli1(:,1:4) clv231(:,1:4)];
cA121 = [cli1(:,1:4) clv121(:,1:4)];
cA141 = [cli1(:,1:4) clv141(:,1:4)];

coef341 = lossfn1a(mu341, tau1)
coef231 = lossfn1a(mu231, tau1)
coef121 = lossfn1a(mu121, tau1)
coef141 = lossfn1a(mu141, tau1)

coefs1 = [coef341 coef231 coef121 coef141];

plot(ct1, cli1(:,5), ct1, cA341*mu341);
plot(ct1, cli1(:,5), ct1, cA231*mu231);
plot(ct1, cli1(:,5), ct1, cA121*mu121);
plot(ct1, cli1(:,5), ct1, cA141*mu141);

%# experiment 2
```

99

```
tau2 = 5e-6;

li2 = lambdae(i2, t2, tau2);
lv342 = lambdae(v342, t2, tau2);
lv232 = lambdae(v232, t2, tau2);
lv212 = lambdae(v212, t2, tau2);
lv142 = lambdae(v142, t2, tau2);

A342 = [li2(:,1:4) lv342(:,1:4)];
b = li2(:,5);
mu342 = A342  b;

A232 = [li2(:,1:4) lv232(:,1:4)];
mu232 = A232  b;

A212 = [li2(:,1:4) lv212(:,1:4)];
mu212 = A212  b;

A142 = [li2(:,1:4) lv142(:,1:4)];
mu142 = A142  b;

cli2 = lambdae(ci2, ct2, tau2);
clv342 = lambdae(cv342, ct2, tau2);
clv232 = lambdae(cv232, ct2, tau2);
clv212 = lambdae(cv212, ct2, tau2);
clv142 = lambdae(cv142, ct2, tau2);

cA342 = [cli2(:,1:4) clv342(:,1:4)];
cA232 = [cli2(:,1:4) clv232(:,1:4)];
cA212 = [cli2(:,1:4) clv212(:,1:4)];
cA142 = [cli2(:,1:4) clv142(:,1:4)];

coef342 = lossfn1a(mu342, tau2)
coef232 = lossfn1a(mu232, tau2)
coef212 = lossfn1a(mu212, tau2)
coef142 = lossfn1a(mu142, tau2)

coefs2 = [coef342 coef232 coef212 coef142];

plot(ct2, cA342*mu342, ct2, cli2(:,5));
plot(ct2, cA232*mu232, ct2, cli2(:,5));
plot(ct2, cA212*mu212, ct2, cli2(:,5));
plot(ct2, cA142*mu142, ct2, cli2(:,5));

%# experiment 3

tau3 = 5e-6;

li3 = lambdae(i3, t3, tau3);
lv343 = lambdae(v343, t3, tau3);
lv323 = lambdae(v323, t3, tau3);
lv213 = lambdae(v213, t3, tau3);
lv143 = lambdae(v143, t3, tau3);

A343 = [li3(:,1:4) lv343(:,1:4)];
b = li3(:,5);
mu343 = A343  b;
```

```
A323 = [li3(:,1:4)  lv323(:,1:4)];
mu323 = A323 \ b;

A213 = [li3(:,1:4)  lv213(:,1:4)];
mu213 = A213 \ b;

A143 = [li3(:,1:4)  lv143(:,1:4)];
mu143 = A143 \ b;

cli3 = lambdae(ci3, ct3, tau3);
clv343 = lambdae(cv343, ct3, tau3);
clv323 = lambdae(cv323, ct3, tau3);
clv213 = lambdae(cv213, ct3, tau3);
clv143 = lambdae(cv143, ct3, tau3);

cA343 = [cli3(:,1:4)  clv343(:,1:4)];
cA323 = [cli3(:,1:4)  clv323(:,1:4)];
cA213 = [cli3(:,1:4)  clv213(:,1:4)];
cA143 = [cli3(:,1:4)  clv143(:,1:4)];

coef343 = lossfn1a(mu343, tau3)
coef323 = lossfn1a(mu323, tau3)
coef213 = lossfn1a(mu213, tau3)
coef143 = lossfn1a(mu143, tau3)

coefs3 = [coef343 coef323 coef213 coef143];
cfs = [coefs1 coefs2 coefs3];
save -ascii coeffs cfs

plot(ct3, cA343*mu343, ct3, cli3(:,5));
plot(ct3, cA323*mu323, ct3, cli3(:,5));
plot(ct3, cA213*mu213, ct3, cli3(:,5));
plot(ct3, cA143*mu143, ct3, cli3(:,5));


%# TOTAL VERIFICATION : LSIM
%# VOLTAGE -> CURRENT

load -force parameters/6bp2
lp = 1e-6*lp; rs = rs;

%# experiment 1

function testexpt1i(lp, rs, ci, cv, ct, num)

  cv341 = cv(:,1); cv231 = cv(:,2);
  cv121 = cv(:,3); cv141 = cv(:,4);

  l1 = lp(1); l2 = lp(2);
  l3 = lp(3); l4 = lp(4);
  l5 = lp(5); l6 = lp(6);

  r1 = rs(1); r2 = rs(2);
  r3 = rs(3); r4 = rs(4);
  r5 = rs(5); r6 = rs(6);

  z1 = [l1 r1]; z2 = [l2 r2];
  z3 = [l3 r3]; z4 = [l4 r4];
  z5 = [l5 r5]; z6 = [l6 r6];
```

```octave
n34 = -conv(z4, (tconv(z5, z2, z3) + tconv(z5, z1, z3) + tconv(z2, z1, z3) + tconv(z6, z3, z5) - tconv(z5,

d1 = (-tconv(z3, z4, z6) + tconv(z4, z2, z6) - tconv(z3, z1, z6) + tconv(z1, z6, z2) - tconv(z4, z2, z3) -

n23 = fconv(z1, z2, z3, z4);

n14 = conv(z4, (-tconv(z3, z1, z6) + tconv(z1, z6, z2) - tconv(z5, z2, z3) - tconv(z5, z1, z3) - tconv(z2,

n12 = tconv(z4, z1, (-conv(z6, z3) + conv(z2, z6) - conv(z2, z3)));

  if num == 1
    plot(ct, ci, ct, lsim(d1, n34, cv341, ct));
  elseif num == 2
    plot(ct, ci, ct, lsim(d1, n12, cv121, ct));
  elseif num == 3
    plot(ct, ci, ct, lsim(d1, n23, cv231, ct));
  elseif num == 4
    plot(ct, ci, ct, lsim(d1, n14, cv141, ct));
  endif

endfunction

cv1 = [cv341 cv231 cv121 cv141];
testexpt1i(lp, rs, ci1, cv1, ct1, 1)
testexpt1i(lp, rs, ci1, cv1, ct1, 2)
testexpt1i(lp, rs, ci1, cv1, ct1, 3)
testexpt1i(lp, rs, ci1, cv1, ct1, 4)

%# experiment 2

function testexpt2i(lp, rs, ci, cv, ct, num)

  cv342 = cv(:,1); cv232 = cv(:,2);
  cv212 = cv(:,3); cv142 = cv(:,4);

  l1 = lp(1); l2 = lp(2);
  l3 = lp(3); l4 = lp(4);
  l5 = lp(5); l6 = lp(6);

  r1 = rs(1); r2 = rs(2);
  r3 = rs(3); r4 = rs(4);
  r5 = rs(5); r6 = rs(6);

  z1 = [l1 r1]; z2 = [l2 r2];
  z3 = [l3 r3]; z4 = [l4 r4];
  z5 = [l5 r5]; z6 = [l6 r6];

  n23 = tconv(z2, z5, ( conv(z4, z6) + conv(z3, z1) + conv(z1, z6) + conv(z1, z4) ) );

  d2 = tconv(z3, z4, z6) + tconv(z1, z3, z6) + tconv(z1, z3, z4) + tconv(z1, z2, z3) + tconv(z5, z1, z3) +

  n34 = tconv(z3, z5, (conv(z4, z2) + conv(z4, z6) + conv(z1, z4) + conv(z1, z6) ) );

  n14 = tconv(z4, z5, (conv(z2, z3) + conv(z3, z6) + conv(z1, z3) + conv(z2, z6) ) );

  n21 = tconv(z1, z5, (conv(z2, z3) + conv(z2, z6) + conv(z2, z4) + conv(z3, z6) ) );

  if num == 1
```

```octave
      plot(ct, ci, ct, lsim(d2, n34, cv342, ct));
    elseif num == 2
      plot(ct, ci, ct, lsim(d2, n14, cv142, ct));
    elseif num == 3
      plot(ct, ci, ct, lsim(d2, n23, cv232, ct));
    elseif num == 4
      plot(ct, ci, ct, lsim(d2, n21, cv212, ct));
    endif

endfunction

cv2 = [cv342 cv232 cv212 cv142];
testexpt2i(lp, rs, ci2, cv2, ct2, 1)
testexpt2i(lp, rs, ci2, cv2, ct2, 2)
testexpt2i(lp, rs, ci2, cv2, ct2, 3)
testexpt2i(lp, rs, ci2, cv2, ct2, 4)

%# experiment 3

function testexpt3i(lp, rs, ci, cv, ct, num)

  cv343 = cv(:,1);  cv323 = cv(:,2);
  cv213 = cv(:,3);  cv143 = cv(:,4);

  l1 = lp(1);  l2 = lp(2);
  l3 = lp(3);  l4 = lp(4);
  l5 = lp(5);  l6 = lp(6);

  r1 = rs(1);  r2 = rs(2);
  r3 = rs(3);  r4 = rs(4);
  r5 = rs(5);  r6 = rs(6);

  z1 = [l1 r1];  z2 = [l2 r2];
  z3 = [l3 r3];  z4 = [l4 r4];
  z5 = [l5 r5];  z6 = [l6 r6];

  n32 = tconv(z3, z2, (conv(z4, z6) + conv(z5, z6) + conv(z1, z6) + conv(z1, z4) ) );

  d3 = tconv(z3, z4, z6) + tconv(z3, z1, z6) + tconv(z3, z1, z4) + tconv(z2, z1, z3) + tconv(z5, z1, z3) + t

  n34 = conv(z3, ( tconv(z1, z4, z2) + tconv(z4, z2, z5) + tconv(z1, z4, z5) + tconv(z4, z2, z6) + tconv(z1,

  n14 = tconv(z3, z4, (conv(z2, z1) + conv(z1, z5) + conv(z2, z5) + conv(z5, z6) ) );

  n21 = tconv(z3, z1, (conv(z5, z6) - conv(z4, z2) ) );

  if num == 1
    plot(ct, ci, ct, lsim(d3, n32, cv323, ct));
  elseif num == 2
    plot(ct, ci, ct, lsim(d3, n14, cv143, ct));
  elseif num == 3
    plot(ct, ci, ct, lsim(d3, n34, cv343, ct));
  elseif num == 4
    plot(ct, ci, ct, lsim(d3, n21, cv213, ct));
  endif

endfunction

cv3 = [cv343 cv323 cv213 cv143];
```

```
testexpt3i(lp, rs, ci3, cv3, ct3, 1)
testexpt3i(lp, rs, ci3, cv3, ct3, 2)
testexpt3i(lp, rs, ci3, cv3, ct3, 3)
testexpt3i(lp, rs, ci3, cv3, ct3, 4)
```

C.3.2 The discrete-time identification method

```
%# get parameter values for the full discrete-time model
%# and cross-validate them

%# this code is written assuming that the voltage
%# probes are configured such that all of the voltages
%# measured are positive when current is injected into
%# node 2 (the rear left corner of the car when viewed
%# facing the car from the front)

clear

%# load data
%# standard v341, v231, v121, v141 sort of stuff

%# define functions

function B = resampleme(A, P, Q)

  B = zeros( (P/Q).*rows(A), columns(A));

  for k = 1:columns(A)
    B(:,k) = resample(A(:,k), P, Q);
  endfor

endfunction

function B = modify(A, P, Q)

  %# subtract the offset in the first 500 samples
  %# and resample at some rate

  range = 1:500;
  B = zeros( (P/Q).*rows(A), columns(A));

  for k = 1:columns(A)
    x = A(:,k);
    y =  x - mean(x(range));
    B(:,k) = resample(y, P, Q);
  endfor

endfunction

dataloadac
```

```
%# a = 50us/div
%# b = 100us/div
%# c = 500us/div
%# d = 50us/div
%# e = 50us/div

vt1a = [v211(:,1) v231(:,1) v341(:,1) v141(:,1)];
vt1b = [v211(:,2) v231(:,2) v341(:,2) v141(:,2)];
vt1c = [v211(:,3) v231(:,3) v341(:,3) v141(:,3)];
vt1d = [v211(:,4) v231(:,4) v341(:,4) v141(:,4)];
vt1e = [v211(:,5) v231(:,5) v341(:,5) v141(:,5)];

vt2a = [v212(:,1) v232(:,1) v342(:,1) v142(:,1)];
vt2b = [v212(:,2) v232(:,2) v342(:,2) v142(:,2)];
vt2c = [v212(:,3) v232(:,3) v342(:,3) v142(:,3)];
vt2d = [v212(:,4) v232(:,4) v342(:,4) v142(:,4)];
vt2e = [v212(:,5) v232(:,5) v342(:,5) v142(:,5)];

vt3a = [v213(:,1) v233(:,1) v343(:,1) v143(:,1)];
vt3b = [v213(:,2) v233(:,2) v343(:,2) v143(:,2)];
vt3c = [v213(:,3) v233(:,3) v343(:,3) v143(:,3)];
vt3d = [v213(:,4) v233(:,4) v343(:,4) v143(:,4)];
vt3e = [v213(:,5) v233(:,5) v343(:,5) v143(:,5)];

vt1 = [vt1a vt1b vt1c vt1d vt1e];
vt2 = [vt2a vt2b vt2c vt2d vt2e];
vt3 = [vt3a vt3b vt3c vt3d vt3e];
vt = [vt1 vt2 vt3];

it = [i1a i2a i3a];




%# characterization data

vt1 = [vt1a vt2a vt3a];
it1 = [i1a(:,1) i2a(:,1) i3a(:,1)];
nt1 = [1 2 3];

vt2 = [vt1b vt2b vt3b];
it2 = [i1a(:,2) i2a(:,2) i3a(:,2)];
nt2 = [1 2 3];

vt3 = [vt1c vt2c vt3c];
it3 = [i1a(:,3) i2a(:,3) i3a(:,3)];
nt3 = [1 2 3];

%# cross-validation data

vx1 = [vt1d vt2d vt3d];
ix1 = [i1a(:,4) i2a(:,4) i3a(:,4)];
nx1 = [1 2 3];

vx2 = [cvs1 cvs2 cvs3];
ix2 = [cia1(:,1) cia2(:,1) cia3(:,1)];
nx2 = [1 2 3];

vx3 = [cvl1 cvl2 cvl3];
```

```octave
ix3 = [cia1(:,2) cia2(:,2) cia3(:,2)];
nx3 = [1 2 3];


%# define functions

function err = absub(mu, v, itest, node)

  a = mu(1:6);

  A = [-1 0 0 1 0 1;
        1 1 0 0 1 0;
        0 -1 1 0 0 -1;
        a(1) 0 0 a(4) -a(5) 0;
        0 0 a(3) -a(4) 0 a(6);
        -a(1) a(2) 0 0 0 -a(6)];

  b = mu(7:12);

  B = -[b(1) 0 0 b(4) -b(5) 0;
0 0 b(3) -b(4) 0 b(6);
-b(1) b(2) 0 0 0 -b(6)];

  itv = zeros(6,1);
  ivec = zeros(6,1);

  err = zeros(size(v));

  for k = 1:length(itest)

    %# compute lagged portion of inductor-resistor voltage
    vvec = ivec(1:4)'*diag(b(1:4));

    %# make RHS for finding the i(k)'s
    itv(node) = itest(k);
    rhs = itv + [zeros(3,1); B*ivec];

    ivec = A  rhs;

    %# assemble rest of voltage vector
    vvec = vvec + ivec(1:4)'*diag(a(1:4));

    %# make the error
    err(k,:) = v(k,:) - vvec;

  endfor

  err = err(:);

endfunction

function err = getabs(mu, v, itest, node)

  m = length(node);
  n = rows(v);

  err = zeros(4*n,m);

  cc = 1:4:m*4;
```

106

```
  for k = 1:m
    err(:,k) = absub(mu, v(:,cc(k):(cc(k)+3)), itest(:,k), node(k));
  endfor

  err = err(:);

endfunction


%# a function to resample the input so that the least squares
%# algorithm converges much faster

%# a similar kludge function to do verification by using
%# absub()

function vpred = abtest(mu, itest, node)

  a = mu(1:6);

  A = [-1 0 0 1 0 1;
        1 1 0 0 1 0;
        0 -1 1 0 0 -1;
        a(1) 0 0 a(4) -a(5) 0;
        0 0 a(3) -a(4) 0 a(6);
        -a(1) a(2) 0 0 0 -a(6)];

  b = mu(7:12);

  B = -[b(1) 0 0 b(4) -b(5) 0;
0 0 b(3) -b(4) 0 b(6);
-b(1) b(2) 0 0 0 -b(6)];

  itv = zeros(6,1);
  ivec = zeros(6,1);

  err = zeros(length(itest), 4);

  for k = 1:length(itest)

    %# compute lagged portion of inductor-resistor voltage
    vvec = ivec(1:4)'*diag(b(1:4));

    %# make RHS for finding the i(k)'s
    itv(node) = itest(k);
    rhs = itv + [zeros(3,1); B*ivec];

    ivec = A  rhs;

    %# assemble rest of voltage vector
    vvec = vvec + ivec(1:4)'*diag(a(1:4));

    %# make the error
    err(k,:) = vvec;

  endfor

  vpred = err(:);
```

```
endfunction


%# do the estimation dance - all parameters apply with a decimation
%# factor of 1/20.

gaussnewton_options("maxiter", 1000);

[thetat1, fvec, info, iter] = lmrecipes('getabs', 1e-3*ones(12,1), vt1, it1, nt1);
norm(fvec), thetat1'
save parameters/thetat1 thetat1

[thetat2, fvec, info, iter] = lmrecipes('getabs', 1e-3*ones(12,1), vt2, it2, nt2);
norm(fvec), thetat2'
save parameters/thetat2 thetat2

[thetat3, fvec, info, iter] = lmrecipes('getabs', 1e-3*ones(12,1), vt3, it3, nt3);
norm(fvec), thetat3'
save parameters/thetat3 thetat3


%# now use those lovely parameters

load -force parameters/thetat1
load -force parameters/thetat2
load -force parameters/thetat3

pw1 = abtest(thetat1, ix1(:,2), 2);
tw1 = vt2d(:)
plot(1:length(tw1), tw1, 1:length(pw1), pw1)

pw2 = abtest(thetat1, ix2(:,2), 2);
tw2 = cvs2(:);
plot(1:length(tw2), tw2, 1:length(pw2), pw2);

pw3 = abtest(thetat2, ix3(:,2), 2);
tw3 = cvl2(:);
plot(1:length(tw3), tw3, 1:length(pw3), pw3);

pw4 = abtest(thetat3, ix3(:,2), 2);
tw4 = cvl2(:);
plot(1:length(tw4), tw4, 1:length(pw4), pw4);

save -mat-binary ch4f2.mat pw1 tw1
save -mat-binary ch4f3.mat pw2 tw2
save -mat-binary ch4f4.mat pw3 tw3
save -mat-binary ch4f12.mat ix1 t2
save -mat-binary ch4f13.mat ix2 cts2
save -mat-binary ch4f14.mat ix3 cts3

%# now get a set of parameters for a different lag; show that they don't
%# work.

clear tek*

load disk1/ascs/tek00003.asc
load disk1/ascs/tek00002.asc
load disk1/ascs/tek00001.asc
load disk1/ascs/tek00000.asc
```

```
load disk1/ascs/tek00023.asc
load disk1/ascs/tek00022.asc
load disk1/ascs/tek00021.asc
load disk1/ascs/tek00020.asc
load disk1/ascs/tek00043.asc
load disk1/ascs/tek00042.asc
load disk1/ascs/tek00041.asc
load disk1/ascs/tek00040.asc


wva = [tek00003(:,2) tek00002(:,2) tek00001(:,2)];
wia = sc*tek00000(:,2);


wvb = [tek00023(:,2) tek00022(:,2) tek00021(:,2)];
wib = sc*tek00020(:,2);


wvc = [tek00043(:,2) tek00042(:,2) tek00041(:,2)];
wic = sc*tek00040(:,2);


clear tek*


load disk2/ascs/tek00001.asc
load disk2/ascs/tek00011.asc
load disk2/ascs/tek00021.asc


wva = [wva tek00001(:,2)];
wvb = [wvb tek00011(:,2)];
wvc = [wvc tek00021(:,2)];


wv = modify([wva wvb wvc], 1, 10);
wi = modify([wia wib wic], 1, 10);
wn = [1 2 3];



%# analyse

gaussnewton_options("maxiter", 1000);

[thetab1, fvec, info, iter] = lmrecipes('getabs', 1e-3*ones(12,1), wv, wi, wn);
norm(fvec), thetab1'
save parameters/thetab1 thetab1


%# use these icky parameters

load -force parameters/thetab1

pb1 = abtest(thetab1, ix1(:,2), 2);
tb1 = vt2d(:);
plot(1:length(tb1), tb1, 1:length(pb1), pb1);

pb2 = abtest(thetab1, ix2(:,2), 2);
tb2 = cvs2(:);
plot(1:length(tb2), tb2, 1:length(pb2), pb2);
```

Bibliography

[1] Paul D. Agarwal. Eddy-current losses in solid and laminated iron. In *AIEE Transactions*, pages 169–181, May 1959.

[2] W.C. Beattie and S.R. Matthews. Impedance measurement on distribution networks. In *Proc. 29th Universities Power Engineering Conf.*, pages 117–120, September 1994.

[3] Philip R. Bevington and D. Keith Robinson. *Data Reduction and Error Analysis for the Physical Sciences*. McGraw-Hill, 2nd edition, 1992.

[4] R.A. Bozorth. *Ferromagnetism*. Van Nostrand, 1959.

[5] J. Brettle and M.W. Baskerville. Electrical bonding in aircraft. In *IEEE International Symposium on Electromagnetic Compatibility*, pages 124–130, 1979.

[6] T.H Fawzi, P.E. Burke, and B.R. McLean. Eddy losses and power shielding of cylindrical shells in transverse and axial magnetic fields. In *IEEE Transactions on Magnetics*, pages 1452–1455, May 1995.

[7] Rolf Johansson. *System Modelling and Identification*. Prentice Hall, 1993.

[8] S.B. Leeb, S.R. Shaw, and Jr. J.L Kirtley. Transient event detection in spectral envelope estimates for nonintrusive load monitoring. In *IEEE Transactions on Power Delivery*, volume 10, pages 1200–1210, July 1995.

[9] Rob Lepard. Power quality prediction based on determination of supply impedance. Master's thesis, Massachusetts Institute of Technology, 1996.

[10] A.V. Oppenheim and R.W. Schafer. *Discrete-Time Signal Processing*. Prentice-Hall, 2nd edition, 1999.

[11] William H. Press, Saul A. Teukolsky, William T. Vetterling, and Brian P. Flannery. *Numerical Recipes in C*. Cambridge University Press, 2nd edition, 1992.

[12] S.R. Shaw, R.F. Lepard, and S.B. Leeb. Desire: A power quality prediction system. In *Proc. 28th North American Power Symp.*, pages 581–587, November 1996.

[13] Steven R. Shaw, Christopher R. Laughman, Steven B. Leeb, and Rob F. Lepard. A power quality prediction system. In *IEEE Transactions on Industrial Electronics*, pages 511–517, June 2000.

[14] Gilbert Strang. *Introduction to Applied Mathematics*. Wellesley-Cambridge Press, 1986.

[15] Gilbert Strang. *Introduction to Linear Algebra*. Wellesley-Cambridge Press, 1993.